DESIGN A CONTROL SYSTEM FOR THE LOW-COST MICRO-MANIPULATOR

A Dissertation

Submitted to the Faculty

of

Purdue University

by

Bo Ji

In Partial Fulfillment of the

Requirements for the Degree

of

Master of Science

August 2019

Purdue University

West Lafayette, Indiana

THE PURDUE UNIVERSITY GRADUATE SCHOOL
STATEMENT OF DISSERTATION APPROVAL

Dr. David J. Cappelleri, Chair

School of Mechanical Engineering

Dr. Raymond J. Cipra

School of Mechanical Engineering

Dr. Song Zhang

School of Mechanical Engineering

Approved by:

Dr. Jay P. Gore

Head of the School Graduate Program

TABLE OF CONTENTS

Page

LIST OF TABLES

LIST OF FIGURES

Figure Page

ABSTRACT

Ji,Bo M.S, Purdue University, August 2019. Design a control system for the low-cost micro-manipulator. Major Professor: David J. Cappelleri, School of Mechanical Engineering.

This thesis report demonstrates a process of designing a control system for a low-cost micro-manipulator fabricated through 3D printing technique. A 3D printed micro-manipulator easily suffers from the problems of unexpected and non-uniform output motions, so a control system is designed to mitigate the external disturbance and improve the output precision of output motions, operation complexity, and motion capability. The overall design process consists of mechanical fabrication, control system design and experimental validations. From the results of validations tests, the 3D printed micro-manipulator is able to generate three dimensional(X, Y, and Z) motorized movements with the travel range at 38 mm in each dimension. Also, it can provide an adjustable output resolution based on different parameter settings in the control system. The minimum step size can reach to 0.76 μm/step. The suggested step size is 2μm/step due to the limitation of perception resolution. The average output precision of the output motion is bounded within 5 μm in the validation tests. In order to improve the user experiences, the suitable operation speed for each dimension ranges from 25 to 50 μm/s. Users can easily control the 3D printed micro-manipulator to do some simple micro-manipulation tasks by manipulating micro-samples through teleoperated or semi-autonomous control provided in the control system. The parts used to build the micro-manipulator are common, off-the-shelf, or 3D printed, so users can easily do the maintenance or repairs on the 3D printed micro-manipulator.

1. INTRODUCTION

In recent years, the micro-technology become a trend in the engineering community [1]. Micro-technology has many advantages on both industrial and research fields. It can provide convenience and benefits on manufacturing or assembling small, highly integrated products due to the reduction on the overall operational, energy and space cost [2]. Currently, Many different examples of micro-technology have been studied and demonstrated. These examples can be divided into two main categories, which are micro-manufacturing and biomedical micromanipulation [3]. A great number of micro-manipulators have been designed and fabricated for the purpose of studying the process of micro-assembling and biomedical cells manipulation. The micro-manipulator become the most indispensable tool in the study of micro-factories, so there is an increase in the demand of the micro-manipulators [4].

Different working tasks and conditions demand different types of micro-manipulator. However, most of the micro-manipulators are built with high-precision, micro-actuators, and high-resolution sensors. Some of the micro-manipulators can provide fully motorized output movements, so they also require high-level control algorithms to regulate the output motions. These characterizations make the micro-manipulators too expensive for some small and medium-sized business. Except for the high cost, the high-resolution micro-manipulator also suffer from the problems of high operation complexity, which is potentially caused by the poor dexterity due to the excessive manual interventions, heavy weight, large volume, and design deflections, so a compromise between the precision, operation complexity and cost need to be achieved. It is necessary to design a micro-manipulator which has the features of low-cost and easy-operation but still can achieve the desired accuracy and motion capability [5].

3D printing is proven to be very reliable and mature prototyping technology, which already evolved into a useful tool in many fields, includes design, manufacturing,

electronics, materials, and business [6]. The three biggest advantages of 3D printing are reducing the manufacturing cost, build time and weight of printed objects. [7] Moreover, the 3D printer makes possible to print the model in an easy and single process [8], so 3D printing technology is considered as a cheap and easy alternative to evaluating and prototyping the micro-manipulator in this thesis report.

Hence, a micro-manipulator need to be designed to achieve four basic goals, which are low fabrication cost, easy operation, high accuracy, and suitable motion capability. This report first propose a mechanical design for the micro-manipulator, and then a control system is designed to improve the output performance of the micro-manipulator. Chapter 2 in this report demonstrates some of the existing benchmarks, and several techniques used in the micro-manipulation. Chapter 3 starts with the mechanical design requirements and then demonstrate the mechanical strategies used in the fabrication process of a low-cost micromanipulator. Chapter 4 shows the methods of designing the control system to motorize the mechanical system and perform feedback perceptual control to improve the output motions. This chapter also demonstrates some useful and convenient features in the control system and how each feature is programmed. Chapter 5 is about performing different kinds of experimental tests to do the characterization and performance validations. Before the validation tests, the fabricated prototype and guiding manual of the control system are presented at the beginning of Chapter 5. The guiding manual is to teach users how to use the control system during the validation tests. The end of this report presents the conclusion of experimental performances and some future works that need to be accomplished to gain more reliable and robust output performance.

2. BACKGROUND AND RELATED WORK

2.1 Micromanipulation

2.1.1 Backgroud of Micromanipulation

The field of Micromanipulation is a critical component in microsystem technology. When compared to conventional manipulation, micromanipulation is more challenging due to the difficulty of analyzing the adhesion force during the manipulation process, so the micromanipulation requires not only high-precision but also the new strategies for manipulation. Adhesion forces, such as van der Waals forces, electrostatic forces, and surface tension force, make the manipulation process highly unrepeatable. Lack of repeatability increase the chances of human interventions. The adhesion force must be mastered or overcame before any micromanipulation. Suitable manipulation strategies and end effectors should be designed to handle the effects of adhesion force [9] [10].

2.1.2 Micromanipulation strategies

The literature from Ref. [10] demonstrates lots of types of micromanipulation strategies. There are two main types of micromanipulation strategies, which are contact and non-contact strategies. Among the listed contact strategies, most of them have gripping operations. Two conventional approaches tweezer-like configure and fixtures configure belong to the micro gripping strategies. Many works have studied how to use micro gripping strategies to achieve micro-assembly. The microgripper is proven to be one of the critical components in the micro-assembly technology by manipulating the micro-objects [11] [12]. However, due to the presence of the adhesion force that is difficult to analyze, these conventional gripping strategies do not perform

well during the operations [13] [14]. The domination of the gravity force during the operation is the precondition for gripping strategies. For example, when a gripper open, the objects should fall due to the gravity forces. This predictable phenomenon leads to many successful griping manipulations in the macroworld. In microworld, the gravity force cannot guarantee to dominate during the manipulations, so the objects may possible remain stuck to the gripper due to the adhesion force after the gripper open [15] [16]. Another literature proposes a pushing manipulation strategy [17] to replace griping manipulation. This idea started from the previous work related to the study on using the pushing manipulation to mitigate the errors due to the friction effects in macroscale objects. The previous study points out that only one point contact between the pusher cannot lead to stable pushing and steering. if there are no further corrective actions taken, the objects tend to rotate pass the pusher. The motions of the object are related to its mass distribution the frictional distributions on its surface, which are difficult to measure by visual perception [18]. Several other works try to estimate and model the friction forces during the pushing dynamics at the macroscale [19] [20] [21], but the model of friction is difficult to analyze due to its nonlinearity. Various friction models were studied in Refs. [22] and [23]. However, these models do not work well in the microworld. With the help of the integration of force and high-resolution optical system, the uncertainties and friction effects can be successful mitigated during the pushing manipulations [15]. In this report, pushing manipulation strategy is implemented to do some simple micro-assembly tasks.

2.2 Benchmarks

Micromanipulators are designed to translate the macromovements from actuators into the microscopic movements. They are widely used in the field of micromanufacturing and biomedical micromanipulation for industry and research purpose. The types of micromanipulators can be distinguished by the number of axes, control methods, resolution of movement, and travel range. A suitable micromanipulator

needs to be purchased or designed based on the particular task requirements. In this section, different types of micromanipautor and their specifications are demonstrated below. The listed micromanipulators are all from the Sutter Instrument, which has developed a good reputation as a manufacturer of high-quality and innovative instruments. Sutter Instrument is also the world leader in both manufacturing micromanipulator and technical knowledge in the field of micro-fabrication.

Figure 2.1 shows a hands control manipulator. It can provide 3-dimensional(X, Y, and Z) movements by manually turning the dials. This hand-control manipulator is designed for a tight environment which requires maximum versatility in a small space. There is a locking mechanism on the top of the manipulator to lock the position of axis and increase the stability. The mechanical drive system is designed with precise racks and pinion to provide drift free and smooth movements [24]. The specifications of MM-33/R hand control micromanipulator are listed in Table 2.1.

Figure 2.1. MM-33/R Micromanipulator [24].

Figure 2.2 shows a large scale hand control manipulator.The biggest difference between MM-33 and MP-85 is that MP-85 can provide not only the coarse movement but also precise movements. The small manipulator mounted on top is the coarse manipulator can only provide the resolution at 0.1 mm. The ultra-fine movements can be achieved with the micrometer mounted at the bottom. This hand-control manip-

Table 2.1. Specifications of MM-33/R Micromanipulator [24]

Travel range(X)	37.0mm
Travel range(Y)	20.0mm
Travel range(Z)	20.0mm
Resolution	100 μm
Price	$1389

ulator is designed for the work tasks that require both coarse and precise movements. There is a rotating mechanism on the base of the manipulator to enable change the orientation of the manipulator. The dual springing of the moment arms can ensure zero backlashes and zero torsion at the precise micrometer [24]. The specifications of MP-85 hand control micromanipulator are listed in Table 2.2.

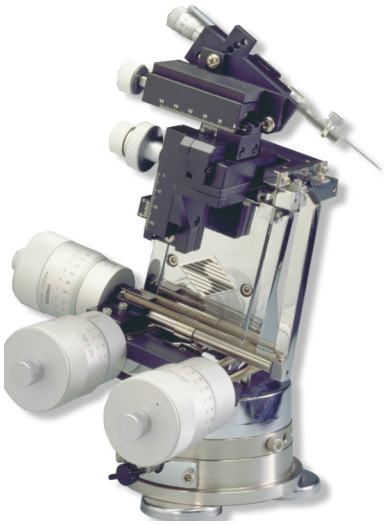

Figure 2.2. MP-85 Micromanipulator [24].

Figure 2.3 shows a motorized micromanipulator. The three-dimensional movements are driven by electric motors. The drive system is designed with the cross-roller bearing slides and worm gear capstan to drive a watch-like mechanism. This motorized manipulator can meet a wide variety of positioning needs by varying the

Table 2.2. Specifications of MP-85 Micromanipulator [24]

Travel range(X)	37.0mm
Travel range(Y)	20.0mm
Travel range(Z)	20.0mm
Ultrafine Resolution	5 μm
Coarse Resolution	100 μm
Price	$6995

operating speeds. The coarse resolution can be achieved at highest speed. The lowest operation speed leads to precise resolution. This manipulator has an extra axle, which is designed to hold the end-effector. The angle of this axle is adjustable depend the users' preference. A controller box call MPC-2000 is available to control the speed and movement of the manipulator. The price of MPC-2000 is $3120 [24],so the total cost of one set of MP-265 micromanipultor requires $9250. The specifications of MP-265 motorized micromanipulator are listed in Table 2.3.

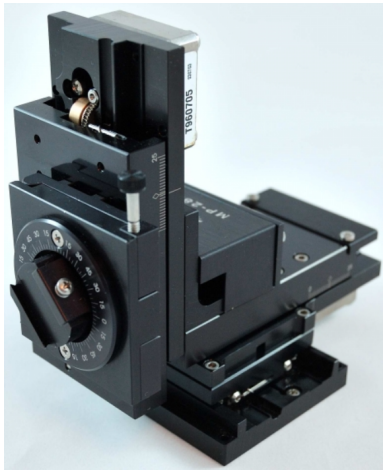

Figure 2.3. MP-265 Micromanipulator [24].

Table 2.3. Specifications of MP-265 Micromanipulator [24]

Travel range(X)	25.0mm
Travel range(Y)	25.0mm
Travel range(Z)	25.0mm
Ultrafine Resolution	0.04 μm/step
Coarse Resolution	0.2 μm/step
Price of manipulator	$ 6130
Price of controller	$ 3120

2.3 Motivation

Although there is a wide variety of micromanipulator available, the cost of them is normally over $1000. Although hand-control manipulators have a relatively low price, these manipulators are not easy to operate and require excessive manual interventions. The motorized manipulators are extremely expensive. Sometimes, one micromanipultor is not enough to achieve the desired output performance, and purchasing several micromanipulators is too expensive for the small and medium-sized business. Also, These high-resolution micromanipulator suffer a common problem, which is hard to replace or repair the parts if the manipulator is broken. Hence, a low-cost micro-manipulator needs to be fabricated, and a control system can be designed to mitigate the potential disturbances from the mechanical system and improve the output precision and operation complexity through the software.

3. MECHANICAL DESIGN

3.1 Design Requirements

For the requirements of mechanical system, the total fabrication cost should be around $500, which is much lower than the price of most of the benchmarks. The fabricated micro-manipulator should be able to provide the three dimensional(X, Y and Z axis) movements. In each axis, the travel range needs to be over 20 mm. The resolution of the design need to be lower than 10 μm/step. Moreover, each part of the design can be easily replaced or 3D printed during the maintenance and repairs. For the requirements of control system, the degree of automation in the design systems should reach the telecontrolled and semi-autonomous level. In both levels, the output movements should be fully motorized. In telecontrolled level, the design needs to execute the user control commands with the implementation of perceptual feedback control. In the semiautomatic level, the design is able to spilt the control commands by generating a set of trajectory point. The design should be easy-operated in both automation levels, so users can easily learn how to operate the design to do some micro-manipulations. During the operation, the control system should be able to mitigate the external disturbance effects and improve the precision of output motions through the perceptual control. In most working environments, the average precision of output motion should be less than 10 μm.

3.2 Design Strategies

The design is designed to provide three dimensional movements, so the whole design can be simplified by separately designing one dimensional component first, and assemble the three dimensional components together to build the whole micromanipulator.

3.2.1 Actuator Selection

In the design requirements, the motions of designed micro-manipulator need to be fully motorized, so the electric motor is the most suitable actuator to drive the micromanipulator. The electric motor has several advantages, like high precision output motion, complete motion control profiles, and compact size. The specifications of the electrical motor, like resolution, smoothness, and speed, can actually determine the output performance of micromanipulator, so there are many requirements on the selection of the electrical actuator. First, the electric motor needs to have a relatively low price($< \$100$). Also, the electric motor can provide smooth and high-resolution output motions at low speed. However, the cheap DC motors suffer from serious cogging torques at the low speed, and cogging torques have large effects on the motors' output performance and controllablity [25]. Developing a method to reduce the cogging torque and smooth the output motion is extremely challenging, which is not the focus in this paper. Some of the high-performance stepper motors with the implementation of the microstepping technique can achieve smooth and precise output motion at low speed, but they are quite expensive($> \$300$). A company called IQ motion control provided a cheap brushless DC motor module which can achieve high resolution and smooth output motion at low speed. A control module attached to the brushless DC motor responsible for compensating the cogging torque effects and performing high precision feedback control algorithm. Many built-in APIs in the control module can perform different levels of position and speed control based on the users' requirements. The specifications of the motor module from IQ motion control are listed in Table 3.1.

3.2.2 Drive System

The next step of design focuses on converting the rotary motions generated from the electric actuator into the linear movements for the end-effector. The feed-screw design is one of the popular mechanisms to convert rotary movements into the linear

Table 3.1. Specifications of GB-2808 motor module from IQ motion control

Resolution	0.022 °
Speed	0.1 rpm
Smoothness	reduce cogging torque by 88 %
Size	3cm × 3.5cm × 3.5cm
Price	$88

movements. There are two general types of feed-screw, which are lead-screw and ball-screw [26] shown in Figure 3.1. The lead screw is a threaded rod with a nut moves parallel with the rod as the lead screw rotate. The ball screw has the matching helical grooves that allow the ball bearings to re-circulate during the rotation. In order to choose the appropriate type of feed-screw, the characterizations and performances of two types of screw need to be explored and analyzed. From the design requirements, the output motions need to be steady and precise, so the performance on output motions is an important criterion to evaluate these two different mechanisms. Both types of the screw can provide steady and smooth movements, however, the lack of self-locking system in ball screw system can lead to unexpected movements, which affect the output accuracy. Also, each ball screw nut cost over $200, which is much expensive than the lead screw nut($30). Although the ball screw nut has higher efficiency and a longer life cycle than the lead screw nut, the lead screw system is still a better choice because of built-in self-locking mechanism and lower cost. [26]. Moreover, There is still room for improvements on the self-locking system. The self-locking system still suffers from a minor back-lashing problem. The backlash problem is caused by that the threads of nut do not fit snugly around the threads of the screw [27]. In order to eliminate the positioning error caused by the backlash, Replacing the normal lead screw nut with anti-backlash nut is a handy solution. For the choice of the anti-backlash nut and lead screw, the size and pitch of threads for nuts and lead screw need to match up perfectly. The lead screw end support is the

last piece of the puzzle in the lead screw system to reduce the friction at the end of lead screw during the operation. The dimension of lead screw end support need to match up with the diameter of the lead screw.

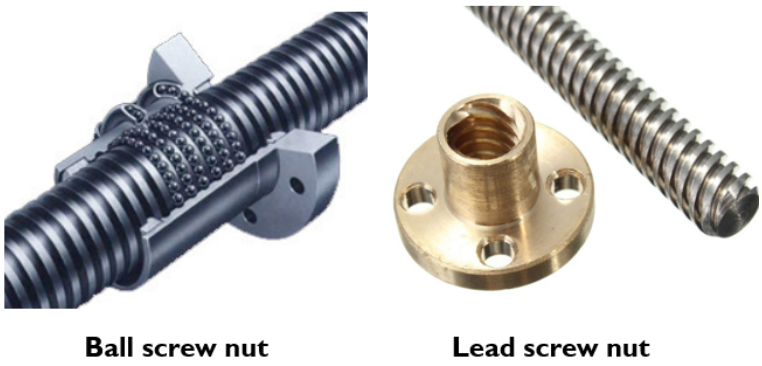

Figure 3.1. The demonstration of two types of feed-screw.

3.2.3 Coupling Connection

The strategy on choosing the appropriate coupling between the electric actuator and drive system is also significant to the design. The motor module from IQ Motion Control company does not have a motor shaft, so 3D printed motor shaft can be designed and mounted on the motor. The shaft coupling is normally used to connected the motor shaft and lead screw. There are two types of couplings, which are rigid couplings and flexible couplings shown in Figure 3.2. The design potentially suffers from the problem of misalignment between the motor shaft and lead screw system. The rigid coupling cannot tolerate any misalignment. Also, the flexible coupling can help absorb the shocks and vibrations [28]. Undoubtedly, the flexible coupling is the better choice of shaft coupling in this design.

Figure 3.2. The demonstration of two types of coupling.

3.2.4 Sliding Rail System

The final prototype is assembled by three dimensional components, so each dimensional component need to be connected with each other by a connector. As mentioned before, the linear movements happen on the anti-backlash nut. The connector need to connect with not only another dimensional component but also the anti-backlash nut. These connections can be easily fixed by several mounting screws. In order to keep the connector and anti-backlash nut relatively static, the anti-backlash nut and the connector need be fixed tightly, so that the connector is able to follow the movements of anti-backlash nut. A guiding rail system needs to be added to stabilize and balance the movement of the connector because the rotatory momentum between the lead screw and the anti-backlash nut can vibrate the whole linear movement and affect the output performance. The vibrations can generate unexpected disturbance which can be inherited in each dimension. The guiding rail system is used to reduce unexpected disturbance and smooth whole linear movements. There are many types of sliding rail system available to choose, however, most of the sliding rails have gaps between the roller and carriage, which can lead to extremely unsteady movement for a micromanipulator. Some of sliding rails with high resolution are extremely expensive. A better solution is to design a low-cost sliding rails with two guiding rods and

several sleeve bearings.The design idea comes from the structure of linear stage. In the design of linear stages shown in Figure 3.3, they normally have two guiding rods to smooth and balance the linear movement. The gaps between the sleeve bearing and a guiding rod can be quite small, so that guiding rod can slide through the sleeve bearing smoothly and steadily.

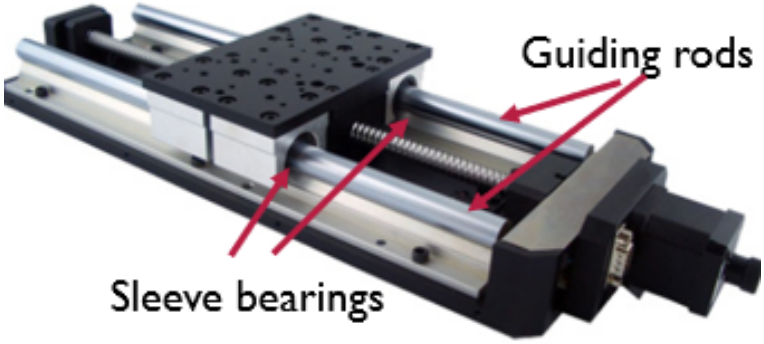

Figure 3.3. The demonstration of linear stage.

3.2.5 3D Printing

Instead CNC machining the structure of each dimensional components, all the structures are 3D printed to lower the total cost and weight of design. As discussed in the introduction, 3D printing is already a mature technology, which can print the prototype in fast and single process. The choice of 3D printing material should provide strong strength and hardness, so that the whole design does not fail during the operation. PLA as a commonly used 3D printing material has good tensile strength and surface quality. The fatigue analysis on the 3D printed parts are demonstrated in following section.

3.3 Specification and Performance

3.3.1 Simulated Prototype Demonstration

The 3D prototype built in SolidWorks strictly follows the design strategies as discussed above. The process of 3D modeling starts with one dimensional component first. Figure 3.4 shown below is the three views of one dimensional component to demonstrate a general appearance of one dimensional component. Figure 3.5 demonstrates how each parts are assembled and connected in the dimensional component. In this figure, different elements are marked by names and different colors to distinguish from each other. The end support, lead screw, anti-backlash nut, flexible coupling, and motor shaft are the major components of the drive system. They are colinear and located at the center line of the design. The anti-backlash is fixed tightly inside the connector by the screws so that the connector is able to follow the movements of anti-backlash nut. A self-designed sliding rails system consists of the two guiding rods and 4 sleeve bearings. Four sleeve bearings are inserted inside the connector, and guiding rods can slide through the sleeve bearings smoothly and steadily. The two ends of guiding rod need to remain fixed and stationary during the operation. This figure can also be used as a supplementary instruction to the section of mechanical design strategies.

The final prototype of micro-manipulator can be assembled by three identical dimensional components together. Figure 3.6 shown below demonstrates the general appearance of the final assembled prototype with an extra probe holder and L-shape connector between x and z dimensional component. In this figure, the three dimensional components and probe holder are labeled. The x and y dimensional component depend on the orientation of the design. A 90-degree rotation in any direction can lead the exchange between x-axis and y-axis. The z-axis always remains unchanged Several theoretical specifications like dimensions and travel range in each dimension can be explored through the 3 view drawing of the final design model. Figure 3.7 and 3.8 shown below demonstrate the separated analysis on the specifications of one

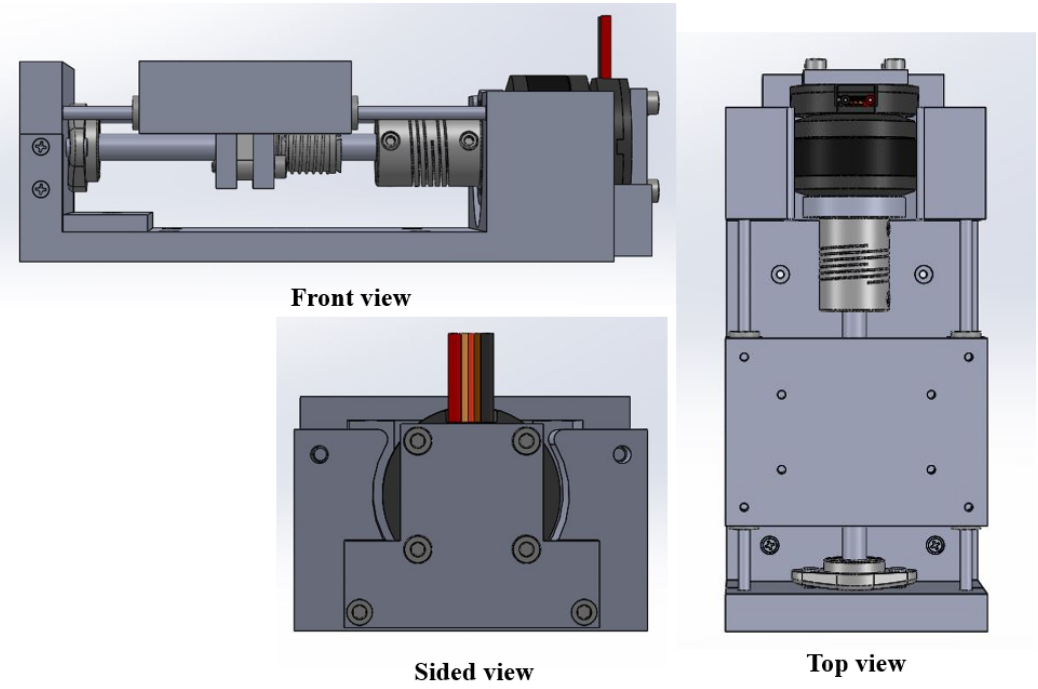

Figure 3.4. The three views of the one dimensional component.

dimensional component and final assembled design. All the significant specifications are listed in Table 3.2 and 3.3 shown below.

Table 3.2. Specifications of one directional component

Length	150.00mm
Width	70.00mm
Height	47.10mm
Travel Range	38.04mm

3.3.2 Specifications and Analysis

The theoretical performance of mechanical design needs to be analyzed to check if the design requirements are satisfied. The theoretical accuracy of the movement

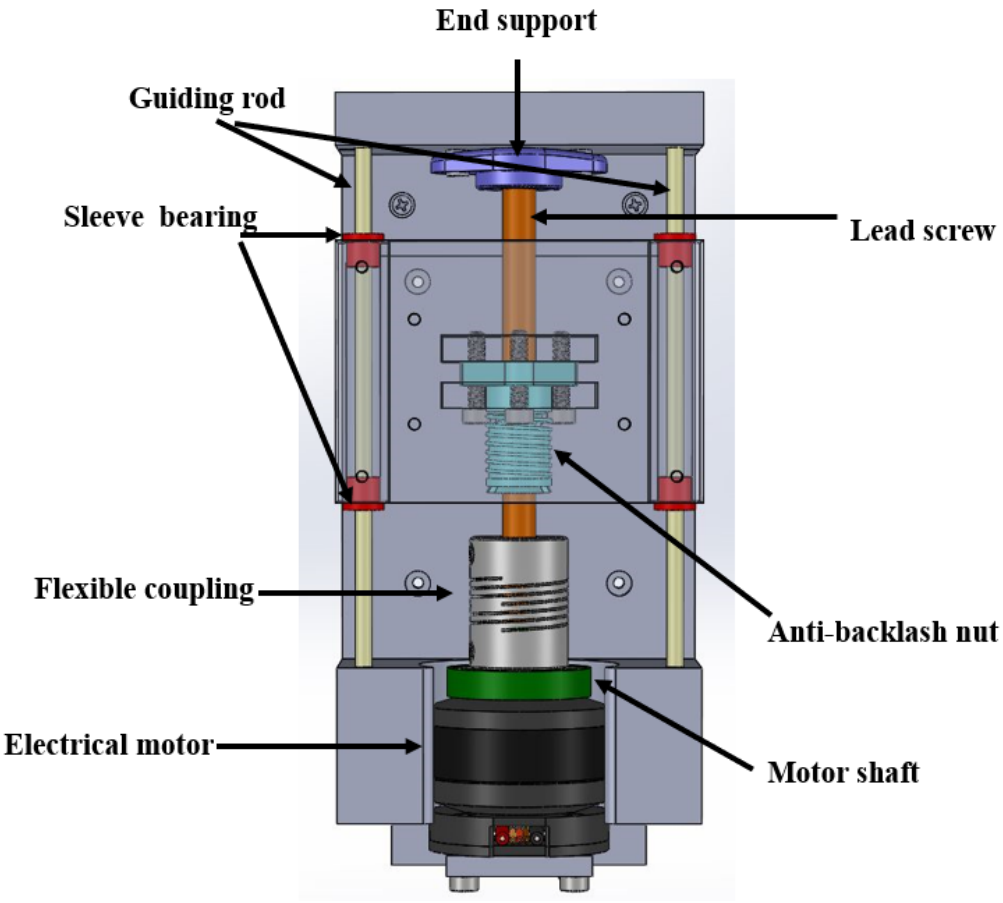

Figure 3.5. The detailed description of design.

Table 3.3. Specifications of Theoretical prototype

Length	238.64mm
Width	150.00mm
Height	184.20mm
Travel Range in each dimension	38.04mm

depends on the resolution of lead screw and encoder of the motor. Table 3.4 and 3.5 shown below are the data sheets of the selected lead screw and electric motor. In these two tables, the travel distance per turn of the lead screw is 1.27mm and resolution of the motor encoder is ±0.00384 rad, so the minimum linear increment

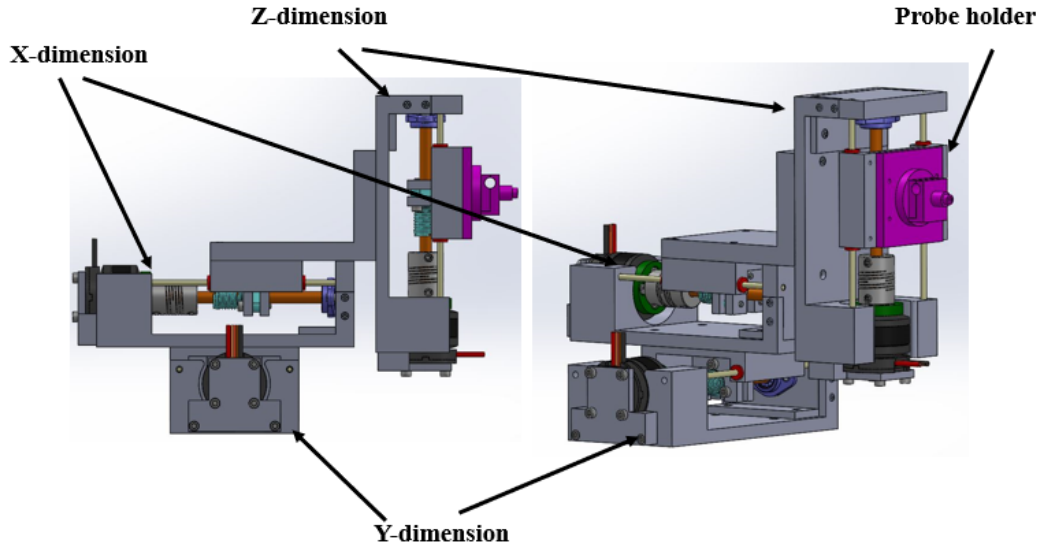

Figure 3.6. The final assembled prototype.

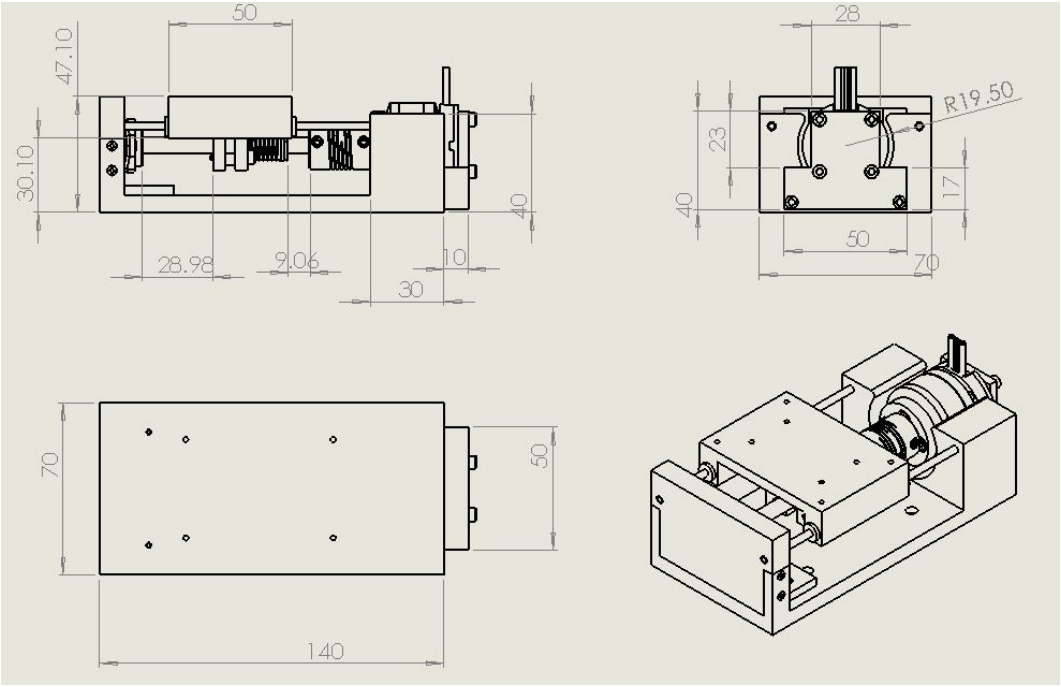

Figure 3.7. The 3-D drawing of one directional component.

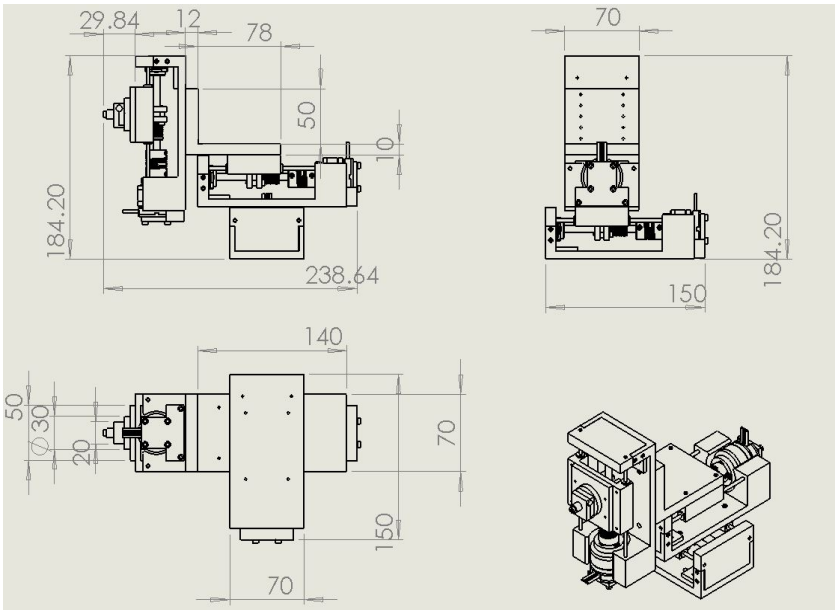

Figure 3.8. The 3-D drawing of final assembly.

can be computed through the Equation(3.1). In Equation(3.1), r represents the rotary angle of the electric motor in radian, C represents the constant value of the linear travel distance of lead screw per turn and D represents the linear movement of the lead screw. The theoretically computed resolution per step is equal to ± 0.76 μm/step, which is less than the required resolution(10 μm/step).

Table 3.4. Data sheet of lead screw

thread size	6.35mm
thread per inch	20
thread angle	29°
length	100mm
speed ratio	1:1
Travel distance per turn	1.27mm
Accuracy for travel distance per meter	$\pm 0.25mm$

Table 3.5. Data sheet of electric motor GB2808

Voltage range	5-17V
Continuous stall current	11.1A
Continuous rotating current	15A
Mass	79g
Maximum Torque	114N mm
Resolution	0.00384 rad

$$D = \frac{rC}{2\pi} \tag{3.1}$$

The required torque needs to be computed to prove that the maximum torque generated by the electric motor is enough to drive the lead screw and workloads. The following equations are used to compute the required torque for the electric motor to drive the load in the design. Figure 3.9 shown below is the sketch of the one dimensional component of the design. The required torque can be computed based on the analysis of this sketch. In Equation (3.3), J_L represents the inertia of the total load and connector int the sketch, M_{W+T} represents the total weight of the load and connector, and P are the lead distance of the lead screw. The formula for computing the inertia of the motor is in Equation (3.4). J_M is the inertia of the electric motor, M_m represents the mass of motor, and r is the radius of the motor. The formula to compute the lead screw inertia(J_s) is the same as the Equation (3.4) with mass of lead screw(M_s) and radius of lead screw (r_s). The total inertia is equal to the sum of the inertia of load, motor and lead screw. The Equation (3.7) and (3.8) demonstrate how to compute acceleration torque and load torque. The acceleration torque is equal to total inertia multiply the current rotary acceleration. In the Equation (3.9),α represents the thread angle for the lead screw, μ is the friction coefficient between the guiding rod and sleeve bearing, and η is the efficiency(reference values is 0.2 to 0.8) of the lead screw. The total torque is equal to the sum of load torque and accelera-

tion torque. In Equation (3.10), a safety factor(K_s) is used to compute the required torque of the motor. Table 3.6 contains several constant parameters, which are useful to compute the required torque in each direction. Table 3.7 demonstrates the load torque, acceleration torque, and total required torque in each direction [29] [30] [31]. The maximum required torque happen in the y-axis, which is located at the bottom of the design. The maximum required torque is around 25 Nmm, which is less than the maximum torque(114 Nmm) the generated by the selected electric motor.

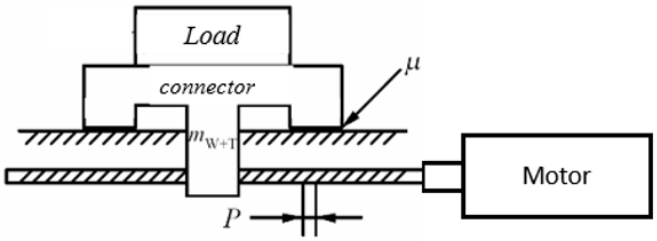

Figure 3.9. The drive system .

$$J_L = M_{W+T}(\frac{P}{2\pi})^2 \tag{3.2}$$

$$J_M = \frac{1}{2}M_m r_m^2 \tag{3.3}$$

$$J_s = \frac{1}{2}M_s r_s^2 \tag{3.4}$$

$$J_T = J_L + J_M + J_s \tag{3.5}$$

$$T_a = J_T\alpha = J_T\frac{\omega_1 - \omega_2}{t} \tag{3.6}$$

$$T_L = \frac{M_{W+T}gP(\sin\alpha + \mu\cos\alpha)}{2\pi\eta} \tag{3.7}$$

$$T_T = T_L + T_a \tag{3.8}$$

$$T_M = K_s T_T \tag{3.9}$$

Table 3.6. constant parameters for design

M_m[g]	$r_m[mm]$	M_s [g]	r_s $[mm]$	P $[mm]$	α [°]	η	μ
90	10	< 100	3.18	1.27	29	0.3	0.4

Table 3.7. Required torque in each direction

Direction	M_{W+T}[g]	$a[rad/s^2]$	$T_L[Nmm]$	$T_a[Nmm]$	K_s	$T_M[Nmm]$
x-axial	831	1	4.5789	5.0395	2	19.2400
y-axial	1353	1	7.4476	5.0608	2	25.0167
z-axial	152	1	0.8385	5.0118	2	11.7007

After computing the maximum required torque in each dimension, the maximum shear stress on 3D printed motor shaft need to be analyzed to check the torsion failure. The shear modulus of PLA is 1287 MPa. The shear stress of a circular shaft can be computed through Equation (3.10). In the equation, τ represents the shear stress acting at the distance ρ from the center of the shaft, J represents the polar momentum inertia of the circular shaft. J can be computed through Equation (3.11) [29] [30] [31]. The maximum shear stress is found by replacing ρ with the radius of the shaft, which is 1.2 cm for each motor shaft. The computed maximum shear stress in each motor shaft is shown in Table 3.8. From the table, the maximum shear stress in Y-axis is way less than the shear modulus of PLA, so the motor shaft can work normally during the operations

$$\tau = \frac{T\rho}{J} \tag{3.10}$$

$$J = \frac{\pi r^4}{4} \tag{3.11}$$

$$\tau_{max} = \frac{Tr}{J} \tag{3.12}$$

Table 3.8. Maximum shear stress in each dimension

Direction	J[m^4]	r[m]	$T_M[Nm]$	τ[MPa]
x-axial	1.628×10^{-8}	1.2×10^{-2}	1.924×10^{-2}	1.418×10^{-2}
y-axial	1.628×10^{-8}	1.2×10^{-2}	2.502×10^{-2}	1.84×10^{-2}
z-axial	1.628×10^{-8}	1.2×10^{-2}	1.17×10^{-2}	8.6×10^{-3}

3.4 Cost of Materials

One of the critical design requirements is to keep the total cost around $500, so a detailed BOM (Bill of Material) is provided below to demonstrate the total cost of the design. The table of BOM consists of the part name, the cost per part, the quantity of the parts, and the total cost of the parts. The final row in Table 3.9 is about how much PLA filament is used to print the structure of the design. The printing cost is the price of one reel of Ultimaker PLA filament. The final total cost is $ 550.65, which is 10 percent higher than the target cost. Except for the electric motor and filament, all other parts can be purchased from McMaster-carr.

Table 3.9. Bill of Material

Part Number	Part Name	Cost per part[$]	Quantity	Total Cost[$]
1	Electric Motor	88.00	3	264.00
2	Shaft Coupling	8.00	3	24.00
3	Anti-backlash Nut	20.23	3	60.69
4	Lead screw	24.72	1	24.72
5	End Supporter	9.70	3	29.10
6	Guiding Rod	15.29	6	91.74
7	Sleeve Bearings	1.95	12	23.40
8	PLA filament	35.00	1	35.00
Overall cost				$550.65

3.5 Advantages and Limitations

Overall, the mechanical system is simple and easy to assembly, because each dimensional component is identical. The structure of the whole prototype is 3D printed with tough PLA, so the workloads in each dimension is light due to small density of PLA material, which helps reduce the friction force on the guiding rail system and required torqued for the electric motor. As analyzed in the previous section, tough PLA also can guarantee the strength and toughness of the structure of the prototype. Compare with using CNC machine,3D printing can not only lower the total cost of building the design but also reduce the workloads during the operation. Although using 3D printing can bring lots of advantages, it still has some limitations, which inevitably have the effects on the performance of output movements. The 3D printed parts always have deviations on the dimensions compared with the desired simulated model in computer. These deviations become more serious, especially on the mounting holes. For example, the deviations on the mounting holes in sliding rail system may compress the sleeve bearings, so that the sliding frictions are not uniform on two guiding rods, which can cause non-uniform and unsteady motions on both sides of the sliding rail system. Also, the deviations on the 3D printed parts may lead to the misalignment outside the tolerance of flexible coupling in the drive system, then the output performance can be affected.

4. CONTROL SYSTEM

Mechanical design shown above is just the foundation of this low-cost micromanipulator. The goals of the mechanical design are just to lower the fabrication cost, provide theoretical high-resolution output and suitable travel ranges. While, the actual mechanical system potentially suffer from some problems, like non-uniform friction distributions and occasionally misalignment problems due to the uncertainties from the 3D printing or assembly deflections. These problems can cause serious the external disturbance which have effects on the output performance of the micromanipulator, while, it is extremely hard to quantify the disturbance in each dimension. A reliable control system becomes the significant and indispensable components in this low-cost manipulator to help mitigate these disturbance effects and improve the precision and smoothness of output motions. The following sections are to demonstrate the details of the designed control system.

4.1 Component and Architecture

The overall control system consists of five main processes, which are image acquisitions, image processing, messages transmissions, position feedback control, and error validations. Figure 4.1 shown below demonstrates the required setups for the whole control system and the relationships between each component. This figure is also useful to help understand the relationship between the five main processes. In the process of image acquisitions, the image frames from the microscope need to be captured. The captured image frames should also be updated on the users' computer screen at the same time to check if the quality of captured frames meets the expectations. If the frames are not available, the control system shuts down automatically and an error message pops up because the rest of processes cannot work

appropriately without the good image acquisitions. In the step of image processing, the control system is responsible for detecting and tracking the tip of the probe, which is the end-effector of the manipulator. After this step, some useful information like tip positions and users' target positions can be extracted from the captured frames. In the messages transmissions process, information generated from the image processing needs to be sent from the computer to a microcontroller through serial communication. The microcontroller is responsible for collecting the messages from the computer and convert the current received messages into the control actions for the motor modules. In order to control the 3-dimensional movements simultaneously and prevent the data corruptions, an Arduino mega 2560 with three extra serial ports [32] is chosen as the microcontroller to send the corresponding control actions to each actuator. Each motor can be controlled by an individual serial port, so that communication process is efficient and safe. In the step of position control, the control actions contain the rotatory direction, target angular position, and rotatory speed for each actuator. The built-in control module uses corresponding control actions to achieve the position controls on each actuator. After actuators finishing the current position control, a trigger signal is sent back from the actuator to the micro-controller to allow the start of the error validation process. After the computer receiving the validation signal from the microcontroller, the control system starts to compute the differences between the current tip position and target position. if the position error is within the predetermined validation threshold, the new control actions will be generated base on the new target set-point and current position, otherwise, the old control actions will be continuously updated until the errors are within the validation threshold.

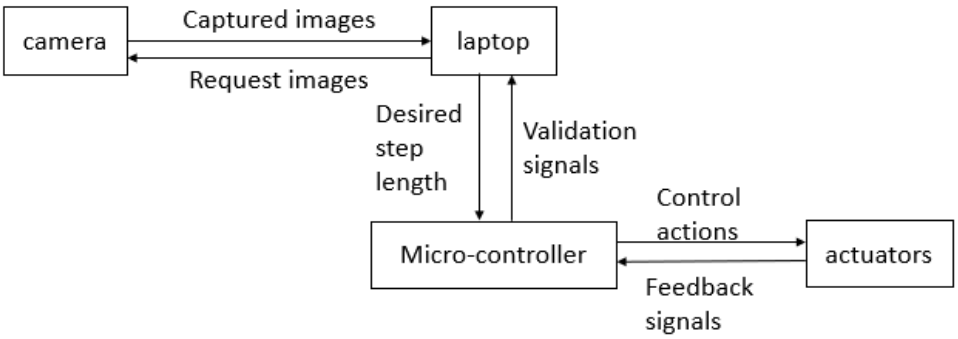

Figure 4.1. The component and architecture of control system .

4.2 Features

4.2.1 Manual Graphic User Interface(GUI) Control

There are several useful features in the control system which can help improve the performance of the micromanipulator. The first feature is a manual GUI control. This feature requires the users to enter the controls input, like rotatory position rotatory speed directional and dimensional selection, to directly control the motions of corresponding control actions. Figure 4.2 demonstrate the appearance of the GUI for the manual mode.The manual mode provides the direct control on the motor module by manipulating the values of rotatory speed, step length for the movement, direction of movement and orientations, so users can easily check the performance from the capture image frames by entering different control actions. Moreover, manual mode can be used as a debugging tool, which can easily find out the reasons for the unexpected performance from the feedback outputs in the captured image frames.

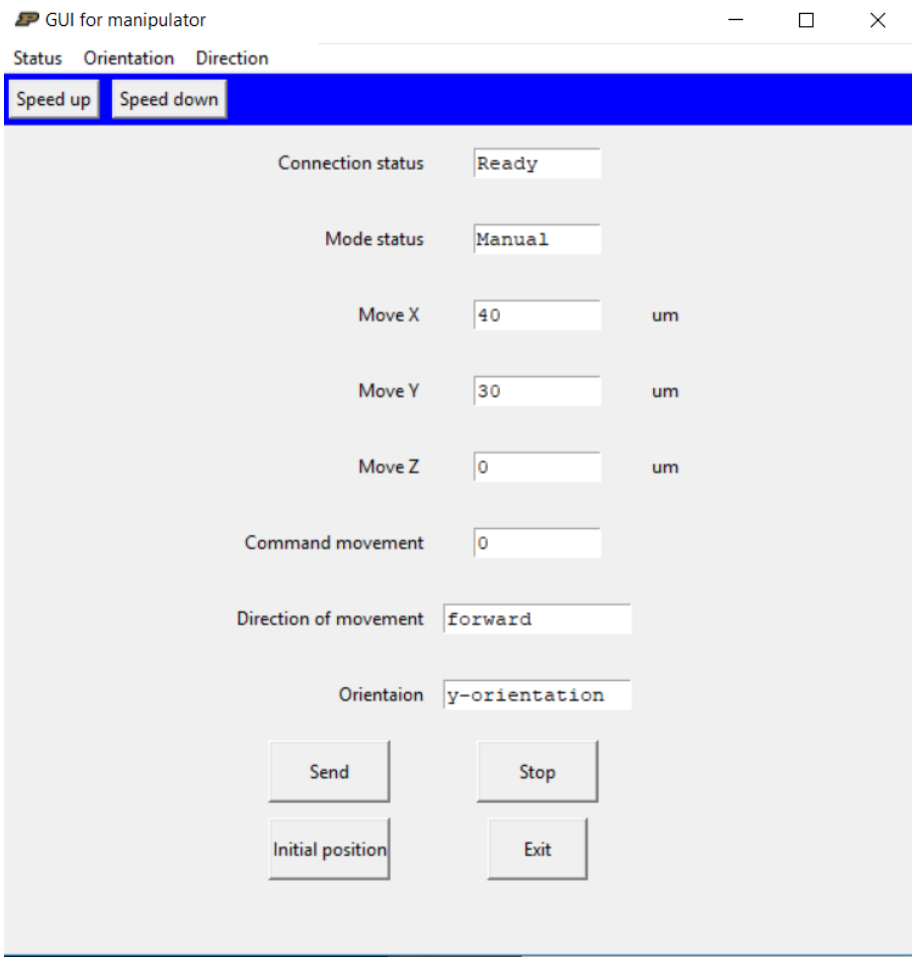

Figure 4.2. The graphic user interface for manual mode

4.2.2 Teleoperated and Semi-autonomous Mode

The second feature is the teleoperated mode, which can automatically generate the control actions base on the feedback position errors and validation signal. In this mode, users can input the commands by clicking points on the captured frames shown on the screen of the computer or pressing the keyboard to generate the target points on the captured frame. The control system can automatically generate the desired control actions to maneuver the manipulator to reach the next target points with perceptual control. The perceptual control includes the built-in control module in the motor and error validation process. This mode is useful to study the performance

of design in the micro-assembly and some other following trajectory tests. Other than the manual mode, the deviations from x and y-direction can be compensated with the help from the error validation process, but the teleoperated control cannot deal with the drift motions happen on the path to the target points, so the semi-autonomous mode can generate a set of way points which can fill the gap between the current tip position and target position. The set of way points can be useful to guide the movement of the tip. Each way point is treated as a target point, so the tip of the probe can move step by step to reach the last target point. The semi-autonomous mode can effectively mitigate the drift motion and deviation on the path to the target positions.

4.2.3 Calibration

The next feature is called calibration function. The presence of this feature is to mitigate the uncertainties from the experimental setup such as inclined camera angle and changed focus of the microscope, which can affect quality of capture frames. Because the focus of microscope and location of camera is fixed manually during the experimental setup, the captured camera views may have sort of deviations and uncertainties. The goal of this feature is to calibrate the deviations and use software to compensate the deviations. The rotation of camera angle and relationship between angular displacement from actuator and pixel length under the current setup need to be calibrated. This feature does not need to be repeated each time when the program starts. If the experimental setups do not change, the calibrated results from the last calibration process still can be used, so the calibration step can be skipped for the convenience.

4.2.4 Error Output

The control system also provides a feature can calibrate the errors from the error validation process in each dimension during the operation. The calibrated error

messages are automatically saved in several external files. With the help of generated errors, the performance of the manipulator can be visualized and analyzed after the end of the tests. The significance of this feature is to provide a systematic and mathematical way to analyze the performance of the micromanipulator through the recorded results during the tests. With the help from the feature of error recording, users can adjust the parameters in control system based on the analyzed results of the output performance.

4.3 Algorithms

4.3.1 Object Tracking

In order to detect the tip of the probe in the camera view, the characterization and specifications of the probe need to be explored. Shape and color detection are two main detection methods in OpenCV. According to the captured frames from the microscope, the lighting conditions may vary because of different experimental setups. The intensity of the lighting source can have a very large impact on the quality of the captured image. The color of tip varies under different intensities of light. Except for the variations on color, there are also some other objects shared the same color to the tip in the captured frame. Using color detection is not a reliable choice to detect and track the tip. For the shape detection, the probe under the camera view does not have a regular shape, so a more robust method needs to be used to accurately to detect the probe. The contour detection is a method belongs to the shape detection, and contour detection can easily find the contour of the probe and keep tracking the contour when the probe is in motion. In order to track the tip of the probe, the apex points of the detected contour can be selected. However, the contour detection only works well if the probe is the only object in the captured frame. The contour detection becomes unreliable when another object shows up and is close to the tip of the probe in the captured frames. The contour detection sometimes put these two objects inside one contour, so that the apex point may not locate at the tip of

the probe. In OpenCV, adding erosion on the contour is a most effective way to separate two objects when they touch each other because erosion method can erode and blur the boundaries between two objects so that two connected objects can be put into separate contours. However, using the erosion method can cause the shift of the tracking point and unstable tracking performance because of the changes on the contours. Figure 4.3 shown below demonstrates the shift of tracking point after applying the erosion method. In the figure, it is obvious that the tracking point shifts downward after the application of erosion. During the micro-manipulation tests, the erosion method causes occasionally unstable tracking, which is shown in Figure 4.4 during the operation. Although adding erosion on the boundaries can help separate two contacted objects at most of the times, this method is still not good due to the poor tracking performance of the tip. The tracking point jumps around during the operations so that the control system has a hard time to do the position control and self-adjustment. In order to avoid these potential issues, another method called template matching can provide a more robust detecting and tracking performance. The theory of template matching is sliding the template image over the captured frames and compare with the template image and path of the captured frame under the template image. The template image is created by taking a screenshot of the part of the tip from the captured frame. if the setups of the system do not change during the operation, this method is more robust and reliable than using the contour method with erosion. Figure 4.5 demonstrates the good performance of tracking with the method of template matching when the two objects are touching each other in the micro-assembly tests. Template matching method also has its limitations, it requires to calibrate the tip of the probe before the initialization of the control system if the setups change. Also, in some complex working environments, the template matching method also may fail to provide accurate detection. The working environments for all the tests in this thesis are relatively simple, so the template matching method works well in all the tests. In the future, template matching still needs to be replaced by the method of semantic segmentation to handle more complex tasks.

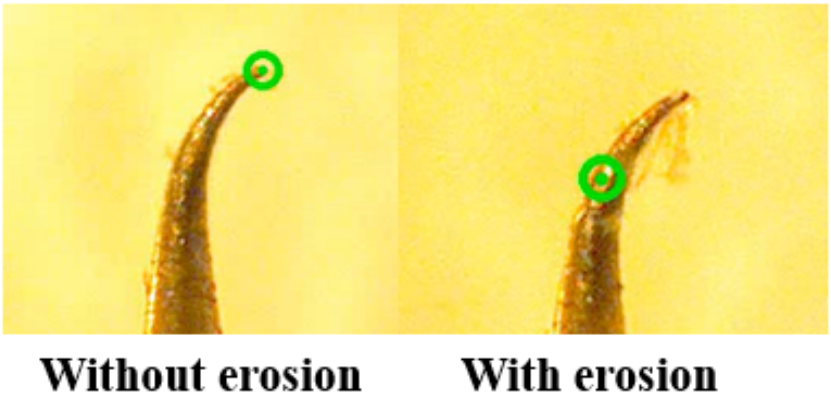

Figure 4.3. The differences after applying the erosion method .

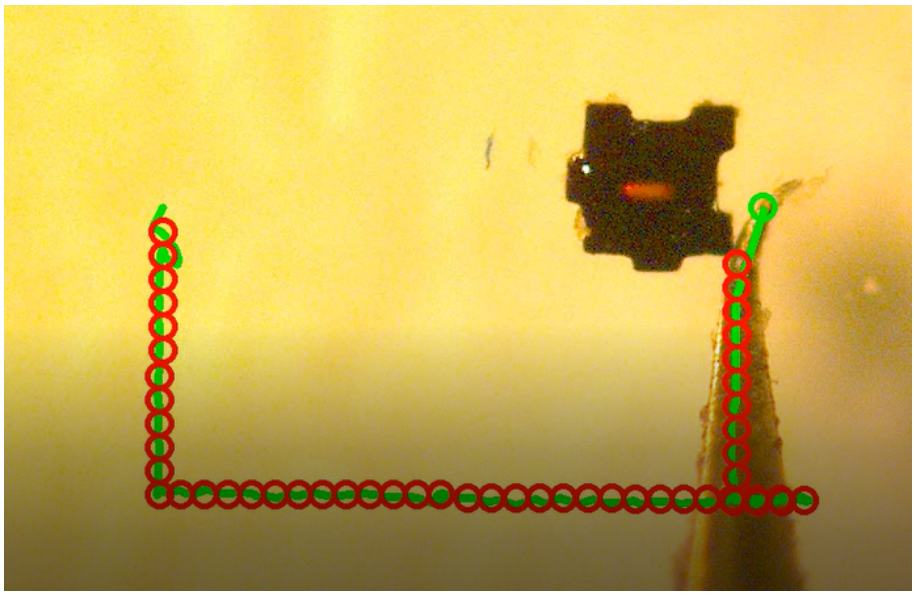

Figure 4.4. The unsteady tracking by using erosion method.

4.3.2 Calibration

The calibration is a significant feature to make sure the control system can operate normally and precisely. As mentioned before, the calibration process can be skipped if the experimental setups do not change. While if the calibration step is not skipped, the calibration starts right after the control system achieving the good

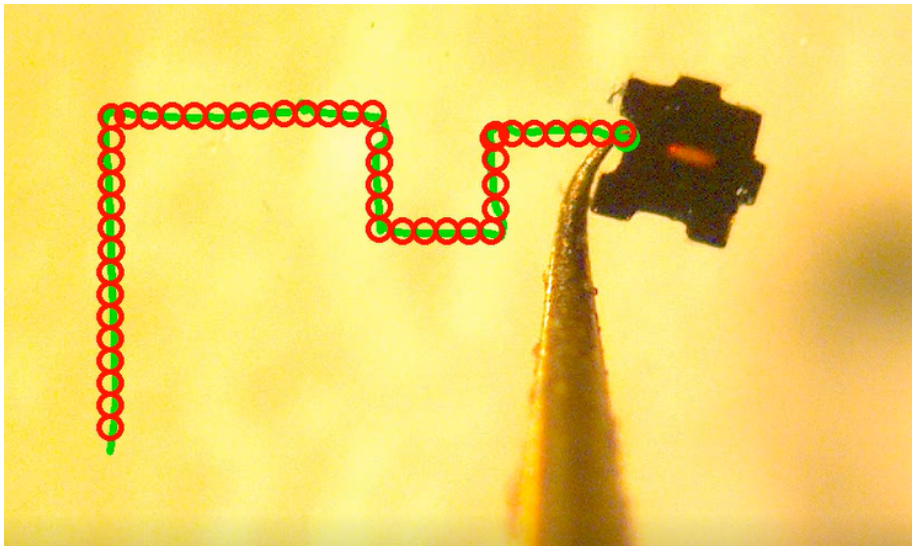

Figure 4.5. The good tracking by using template matching.

tracking results. The calibration is an automatic process consists of two major steps, which are camera angle and rotary displacement calibrations. The angle calibration requires help from the calibration slide. Figure 4.6 shown below demonstrates the scale of calibration slide. The total length of the marked division is 1000 μm so that each small division is 100 μm. The marker division can be useful to find out the conversion between the actual length of movement and pixel length. Before the camera view adjustments, the captured figure on the left side looks like slightly inclined. The rotation angle can be computed by using trigonometric functions through two points on the calibration slide. Users need to click two points on the captured image frame, and the two points need to span 1000 μm, so the control system can easily compute the current perception resolution by measuring the span of the pixel. The perception resolution in current setup is around 2 μm/pixel.After having the rotation angle and perception resolution for the camera view, the status on the left side of the figure can reach to the status on the right side by counter-clockwise rotating 2.23 degrees as shown in the figure. The camera view adjustment and perception resolution processes are performed automatically after have the rotation angle and the span of the pixel. In the step length calibrations, micro-controller starts to send the control actions

with different rotary displacement for the corresponding actuator. The rotary displacement is incremented as each control action finishes. For example, the first step is one-tenth of one revolution, the second step is two-tenths of one revolution, and so on. The calibration for one dimension finishes as the number of increment is equal to the predetermined number of step. After each step, the feedback signal is sent back to the laptop through the serial communication, so the control system can record movement in pixel length under the microscope. The actual movements in micrometer can be computed by using the conversion between pixel and micrometer, which is easily computed with the help from the calibration slide. Figure 4.7 demonstrates the calibrated results in x and y dimension. Due to the limitations of the microscope, the microscope can only capture x and y dimensional movement is this experimental setup. The z dimensional calibration shown in next chapter is performed with a different experimental setup. The deviations in each dimension are plotted in the red line, and the maximum deviations in x and y dimensional movement are 39 and 46 μm. The relationship between the output movement and rotary movement is quite linear, which prove the anti-backlash nuts work well in the mechanical system.

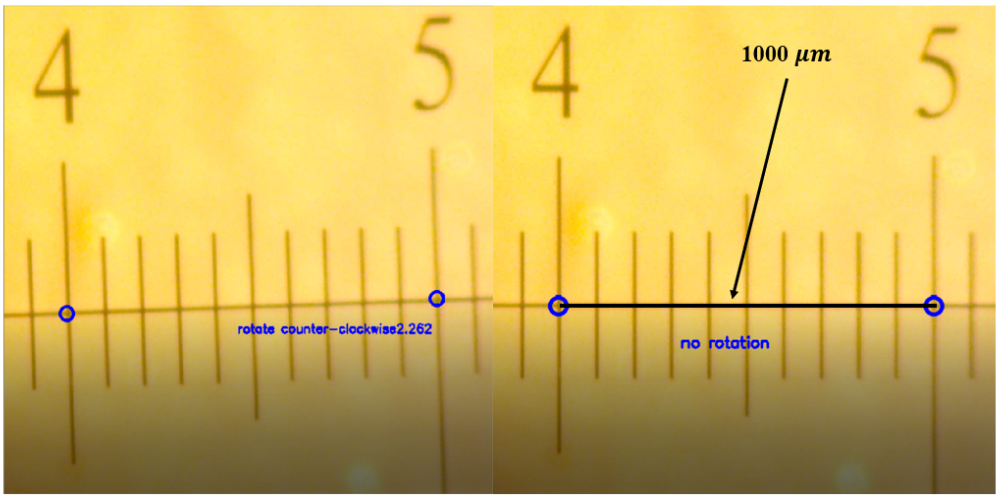

Figure 4.6. The angle calibration and adjustment.

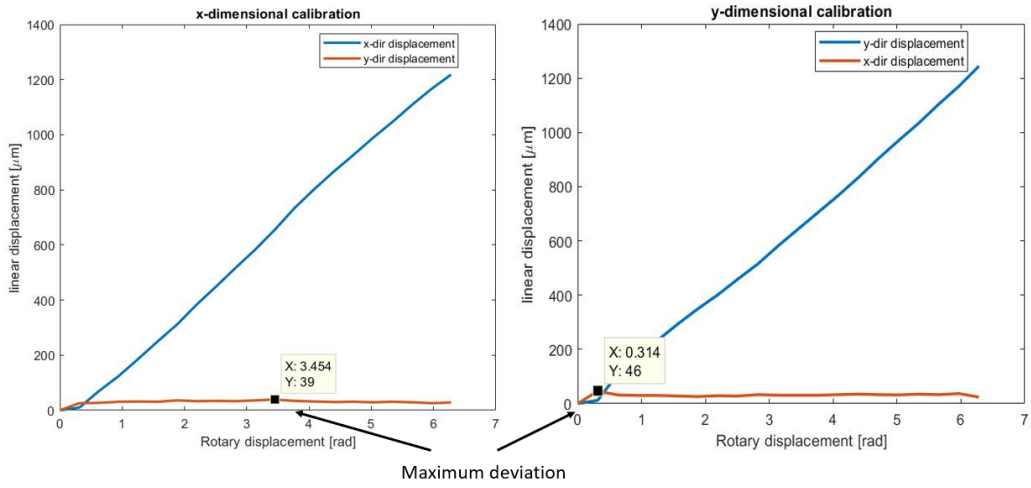

Figure 4.7. The calibration plot from x and y dimension.

4.3.3 Way Points Generation

Way points generation is the key component in the semi-autonomous mode. In order to guide the movements between the target point and current tip position, the way points can be useful to smooth the movement and prevent the tip drifting away from the path. User can tune the gap (default 40 μm) between each way points. If the difference between the target set-point and current position is larger than the gap between way points, the number of way points between the current position and target position can be computed by diving the difference distance by the gap distance. Then, the way points automatically fill the space between the target position and the current position. These way points are very useful to guide the movement of the tip. Figure 4.8 demonstrate the improved performance on output movement with the generation of way point.

4.3.4 Error Validation

The best method to achieve position control is using feedback control, however, the actuator has its own built-in control module which cannot be interrupted send

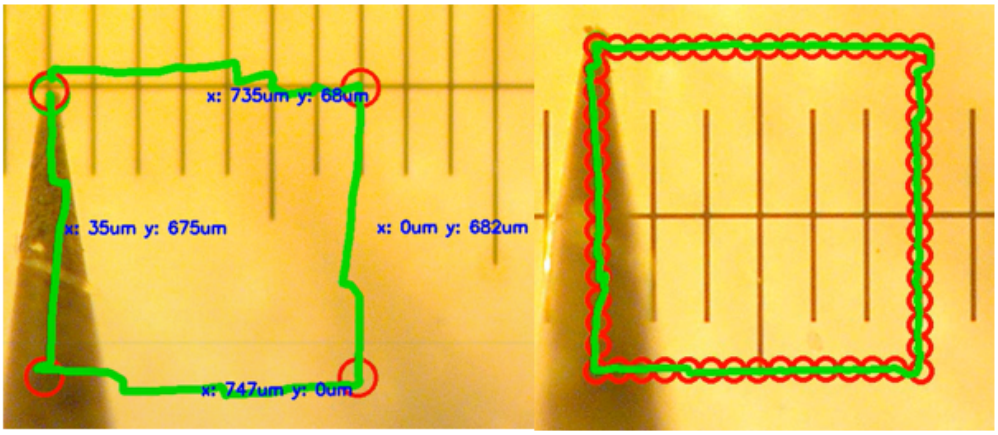

Figure 4.8. Improved performance with the generation of way points.

the feedback signals back to the microcontroller during the operation. Although this built-in control module has an internal feedback control, which can achieve accurate position control, the internal feedback control cannot compensate the external disturbance effects from the mechanical system, so another external feedback control is required to mitigate the external disturbance effects and achieve the high-precision position control. The external feedback control functions as an error validation. After the end of each control action, the control system computes the position error and feeds these errors into the process of validation. There is a pre-determined validation threshold (5 μm) to check if the errors are within the threshold or not. The adjustments need to be continuously performed until the position error is lower than the validation threshold. Because of the existence of the disturbance and deviation, the potential overshoot on the output movements can lead to repeated adjustments at the target position. In order to reduce the possibility of repeated adjustments, a scaling factor can be applied to the position error. Instead of directly converting the position errors into the control actions for the actuators, a scaling factor(less than 1) is used to scale down the control actions for the actuator. The output still can reach the target set-point because of the existence of the error validation process. In the process of

validation, a new scaled position error needs to be remeasured and converted to the new control actions until the position errors reach the validation threshold. Because the scaling factor is less than 1, the probability of excessive adjustments and overshoot is lower than before. Figure 4.9 explains the relationship between each process to provide a better understanding of the logic behind the design of the control system.

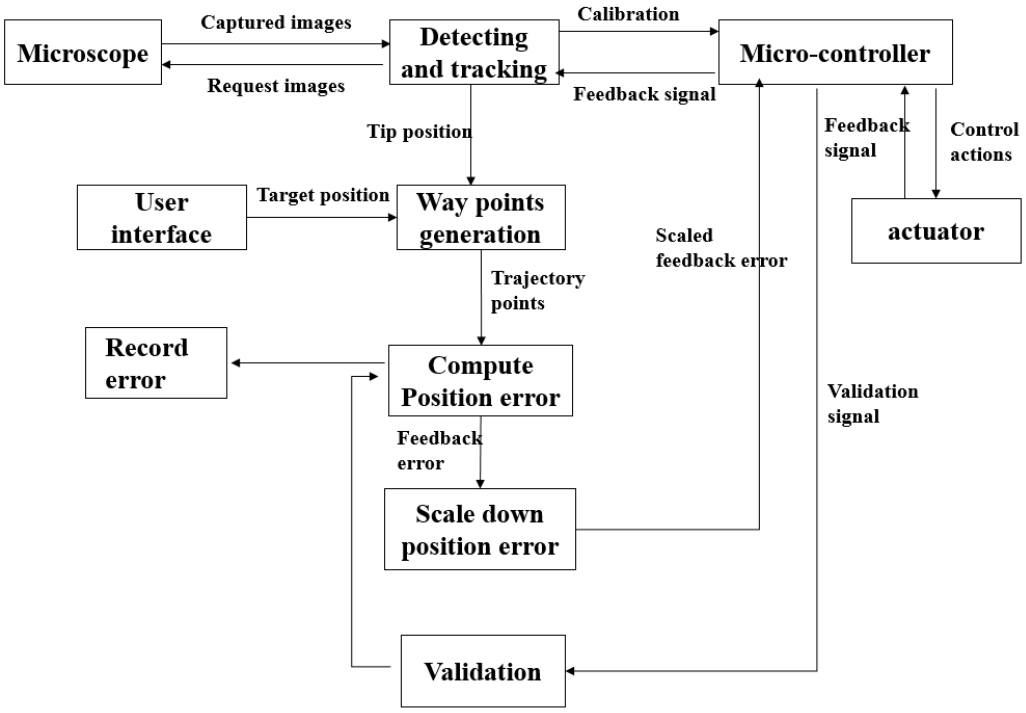

Figure 4.9. The logic behind the control system .

4.4 Limitations

As the logic diagram shown above, the error validation step needs to wait for two periods of serial communications. The micro-controller only can send the validation signal back to the laptop until the built-in control module in the actuator finishes the current control command. Then, the actuator needs to wait for the next control commands, during the waiting, the actuator stays idle, so the actuator cannot respond

fast enough to the sudden unexpected movement due to the disturbance, for example, the tracked object start to drift away from the path. Although the position of the tip can finally be corrected to its desired path, the output precision of design is affected by the time delay in the control system.

Another limitation is caused by the built-in control module in the actuator. Although the control module can generate accurate results, the control module cannot take any control input during the motions. The new control input should wait in the buffer, so the control module is only considered as an accurate open loop control. Although an external validation feedback loop can minimize the potential deviations or uncertainties. the built-in control module is still an unstable factor which may have effects on the performance.

5. EXPERIMENTAL VALIDATION AND PERFORMANCE TESTS

5.1 Experimental Setup

The prototype of the design is built and assembled by following the design strategies. Figure 5.1 shown below demonstrates the appearance of the z-dimensional component with the probe holder. Because each dimensional component is identical in design, the z-dimensional component can be used as an example to demonstrate each piece of this component. The structure of the prototype is close to the simulated design in Figure 3.5. In this figure, each element in the whole component is labeled. Unlike the simulated results in Figure 3.5, the sleeve bearings are deeply mounted inside the connector, so they are invisible in Figure 5.1. The whole blue structure is 3D printed with PLA material. After building the one dimensional component, three identical dimensional components can be connected to each other through the connectors and screws.Figure 5.2 demonstrate the final assembled three-dimensional prototype. The final assembled prototype need to be fixed tightly to the metal pegboard by a 3D printed mounting fixture. Next step is to validate the dimensions of the final prototype with the dimensions from the simulated model. The measured dimensions of the actual prototype are listed in Table 5.1. The measured results are quite close to the simulated prototype in SolidWorks. After the validation of the assembled prototype, the prototype is ready for some experimental tests. The overall experimental setup consists of an assembled prototype, a lighting source, a power supply, a glass holder, a microscope, and a camera holder. Figure 5.3 demonstrate the locations of each component. The assembled prototype is fixed tightly to the metal pegboard to reduce the vibrations during the operation. A probe holder need to fix the probe tightly, so the movement of the probe is steady during the operation. The location of the glass holder depends on the location of the tip of the probe. The

glass holder need to be placed right beneath the tip and fixed by mounting screws to the pegboard. A slide of glass is placed on the top of the glass holder. In order to improve the quality of the captured frame in the microscope, one sheet of white paper can be placed underneath the glass. The lighting source is another important factor can vary the quality of the captured frame, so enough lights can be provided on the glass holder. In the figure, the lighting source is facing the glass slide. The location of the camera holder is the last thing to determine because the location of the camera holder need to make sure the microscope can detect the tip of the probe. The location of the camera is movable on the metal pegboard. Once the tip of the probe is captured by the microscope, the camera holder can be fixed by mounting screws. The orientation of the microscope needs to be adjusted to make sure the probe is upright in the captured frame. Before the experiment, each motor needs to be manually rotated several rounds to check if the motor may potentially get stuck at some points because of some mechanical reasons. After everything is set appropriately, the power supply can be turned on. There are no constraints on the locations of the power supply unless it does not interfere with the operations of the control system. The output voltage should be less than 13 voltages to protect the electrical motors. Operation manual of the control system shown in Table 5.2 need to be checked before performing any tasks. In this table, each input key has its own function and requirement. There are only two mandatory input keys in this control system. As introduced before, the calibration process is a mandatory process if the experimental setup changes. The control system needs to know if the calibration process needs to be performed. Input key s means that the calibration procedure can be skipped because the experimental setup does not change. On the contrary, Input key c means that the calibration need to be performed due to the changes on the experimental setup. One of the input keys must be entered to inform the control system about next status, then some further tasks can be performed. The status of calibration is either skipped or performed.If the control system does not have any statuses of calibration during further operations, the error message pops up and control system should be

shut down. Input key r means the start of the recording, and an external video file is generated after the stop of the control system. Input key t decides whether to print the length of each step on the output frame. The input g,y, and p are useful input commands for the experimental validation tests. They can create the rectangular, circular, and P trajectory for the control system to track. The sizes of these trajectories are predetermined before the initiation of the control system. The rest of numerical inputs belong to the online keyboard control, which can continuously send commands to manipulate the tip positions.

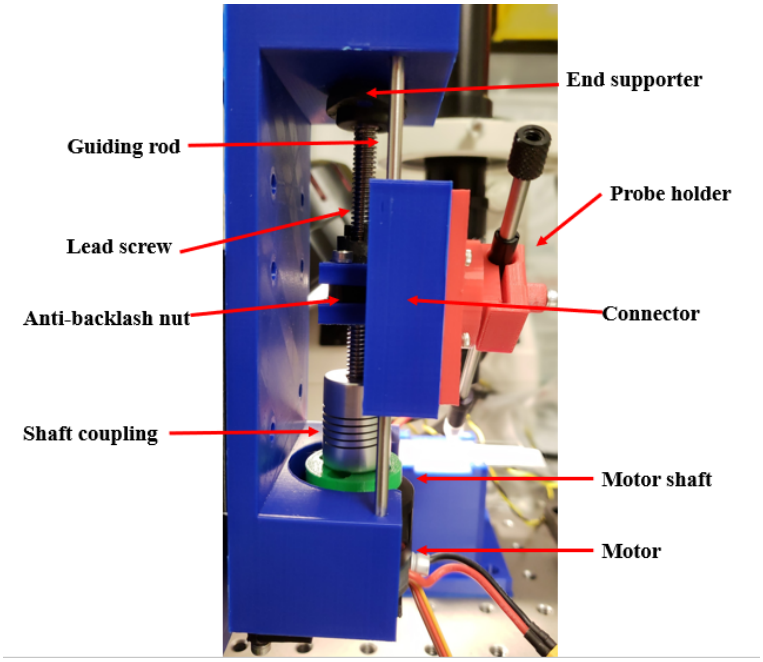

Figure 5.1. Z-dimensional component in the Prototype.

Table 5.1. Specifications of assembled prototype

Length	239.20mm
Width	150.80mm
Height	183.80mm
Travel range in each dimension	38.10mm

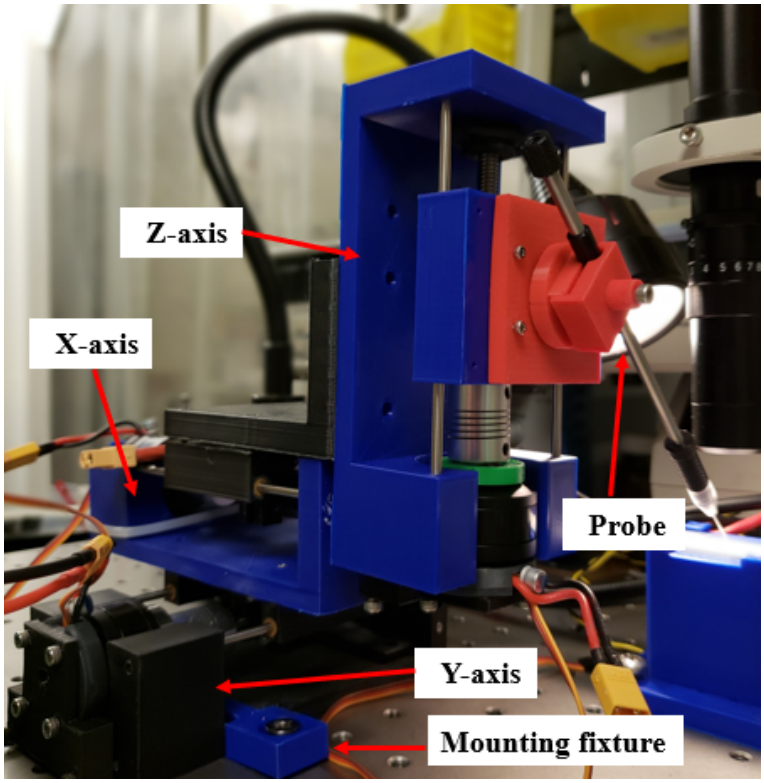

Figure 5.2. Final assembled prototype.

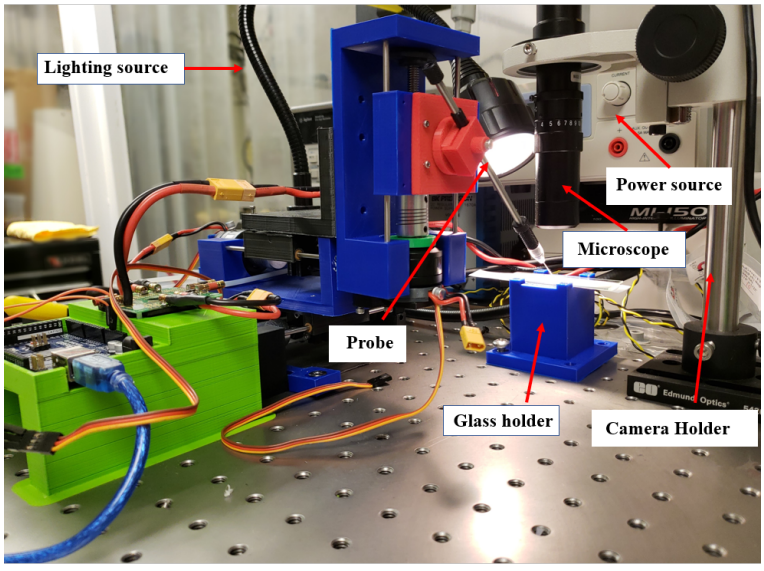

Figure 5.3. Demonstration of experimental setup.

Table 5.2. Operation manual of control system

Keys	Command	Requirement
c	Perform a calibration process	Mandatory
s	Skip a calibration process	Mandatory
r	Start to record	Optional
t	Show the texts on frames	Optional
g	Create a square trajectory on frames	Optional
y	Create a circle trajectory on frames	Optional
p	Create a P shape trajectory on frames	Optional
5	Generate a target point right above the tip	Optional
4	Increase the step size	Optional
6	Decrease the step size	Optional
1	Generate a target point on the left side of tip	Optional
2	Generate a target point right under the tip	Optional
3	Generate a target point on the right side of the tip	Optional

5.2 Z-dimension Validation

From the section of experimental setups, the microscope only can capture two-dimensional movements(X and Y). The z-dimensional movements can only change the clarity of the tracked object because lifting up and laying down the probe lead to the changes on the focus of the microscope. Both directional movements can lead to changes in the clarity of the tracked probe tip. Figure 5.4 shown below how z-directional movements change the clarity of the tracked object in the captured frame. After the z-dimensional movement, the probe in the captured frame is quite blurred. The tracking algorithm is hard to locate the tip of the probe. The consequence is expected because the microscope loses its focus on the probe after the occurrence of the z-dimensional movements. While the changes on the clarity of the probe cannot help

the calibration on the z-dimension. An extra camera holder is 3D printed, which can hold the microscope horizontally so that the microscope can capture the z-dimensional movement. The printed camera holder is only designed for the z-dimensional calibration, and it is not in the actual experimental setup. From the calibration results shown in the section of the control system design, the output movements in both x and y dimension suffer the problem of drift, so the z-dimensional movement cannot be a straight line because of external disturbances from the mechanical design. The deviations from the x and y dimension can be compensated through the validation process. The movement in the z-dimension only can lead to failure of the tracking algorithm, so the validation process cannot compensate the deviations generated from z-dimension. In order to avoid contacts with other objects during the z-dimensional movement, the maximum deviations in the z-dimensional movement need to be calibrated. Figure 5.5record the calibration results in both clockwise and counter-clockwise directions. Because the limitation of the 3D camera holder, the calibrated movement length range from -2500 μm to 2500 μm. The purpose of Figure 5.5 is to show the movement in Z-dimension also suffer from the problem of drift. In this figure, several points in the trajectories are labeled to show the moving distance in x and z dimensions. All the label distance are measured by the difference between the starting point and marked points. The starting points for both cases are located at the bottom of the figure. Each point of trajectory are all recorded in the external files to explore the maximum deviations after the calibration. Table 5.3 demonstrates the maximum deviations in different lengths of z-dimensional movements. The maximum deviations in two different directions are 148 and -121 μm. According to the results of maximum deviations, if this design is assigned to do some tasks involve some z-dimensional movements, the tip needs to keep at least 150 μm away from the other objects to avoid any physical contacts.

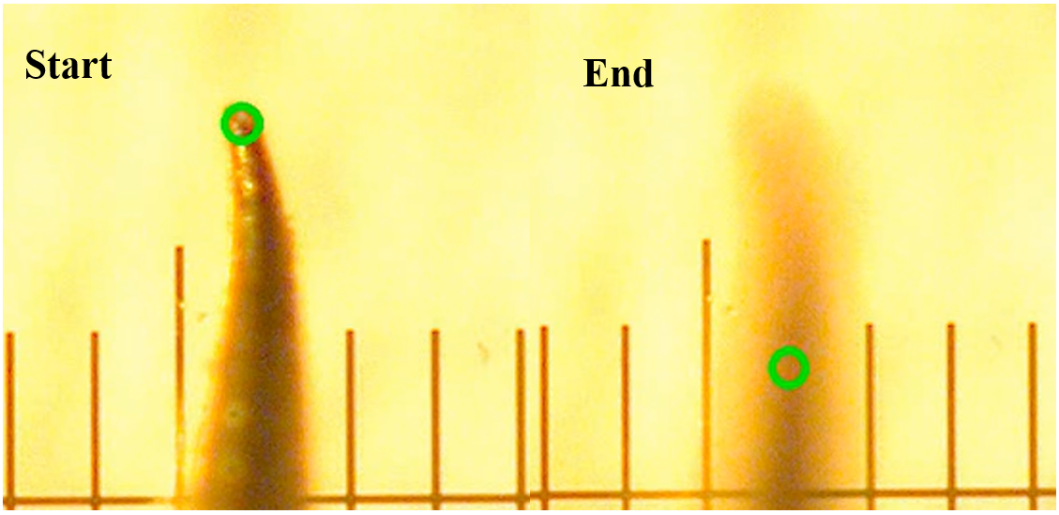

Figure 5.4. The impact of Z-dimensional movement.

Table 5.3. Calibration of maximum deviations in Z-dimensional movement

Direction	500[μm]	1000[μm]	2000[μm]	2500[μm]
Move down	95	105	148	148
Move up	-82	-82	-121	-121

5.3 Resolution and Precision Validation

The theoretical resolution computed in mechanical design section is equal to 0.76μm/step, and this value needs to be validated through several tests in this section. The tests are limited by the perception resolution, which is 2μm/pixel measured in the calibration step, so the test is designed to count how many steps are required to finish 100 μm movement measured by the calibration slide. Figure 5.6 shows the how validation tests are performed. Table 5.4 shows the measured results in five trials of test. Although the computed results are quite close to the theoretical resolution value, the computed result cannot be used to validate the resolution, because this test can not quantify and guarantee that the length of each step is the same due to the limitation of perception resolution. These validation tests can only compute the

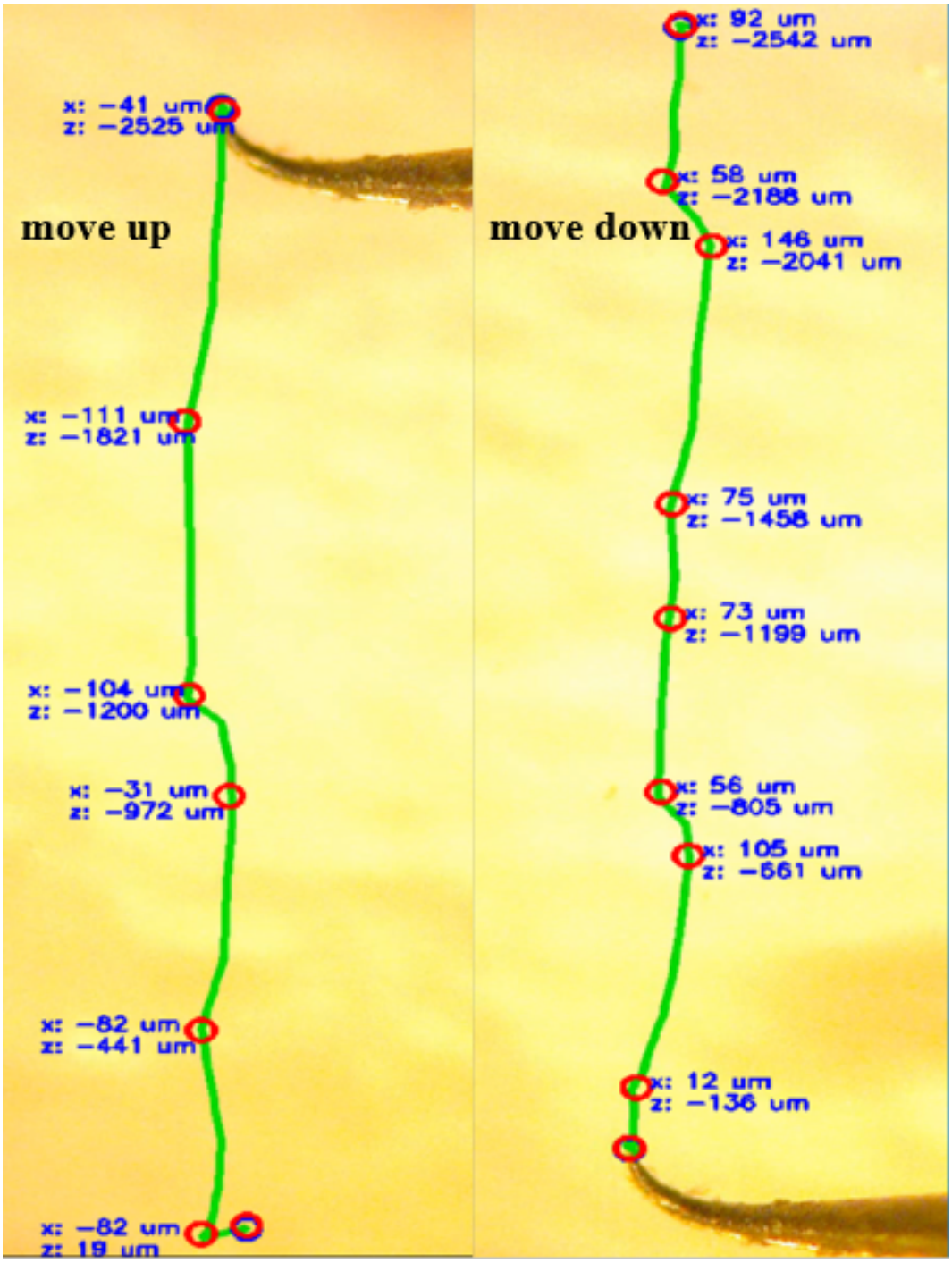

Figure 5.5. The calibrated results of z-dimensional movements.

average minimum step length for the micromanipulator. After the validation of resolution, the actual precision of output movement with perceptual control needs to be

validated. As the discussion in the control system before, the precision of the output movements depends on the validation threshold (default 5 μm), so, theoretically, if the position errors in each dimension are larger than 5 μm, the error validation process starts to adjust the tip position.The output precision of the design depends on the output position errors during the operation. Also, the value of validation can vary depending on the experimental setup and requirements from work tasks. In this section, several experimental tests are performed to explore the relationship between the validation threshold and output precision. The experimental tasks contain different sizes and shapes of trajectory. The experimental tests can be divided into two main types, which are tests of tracking square and circular trajectory. Table 5.5 and 5.6 demonstrate the results of two different types of trajectory tests. From both tables, the average of the experimental position errors are less than 2 μm, and standard deviations of the experimental position errors are less than 1 μm. The maximum position errors in both types of tests are a little higher than 5 μm, which is the default threshold of the error validation. The validation process performs well when the position error is over the threshold, so users can tune the value of the validation threshold to manipulate the precision of the output motion. The default 5 μm is concluded by the results from many experimental tests. Table 5.7 and Figure 5.7 shown below are the demonstrations of how thresholds affect the precision of the output movement.For the current experimental setup, The threshold value should range from 1 to 10 μm, because the larger threshold only has bad effects on the output performance. From the results shown in Table 5.7, the average position error is bounded within 5 μm when the threshold is between 10 and 1μm. The average position can represent the overall output precision. Moreover, it is obvious that when the threshold is less than 5 μm, the validation starts to stop improving the precision of the output motion. Three potential reasons are the limitations of the experimental setup, time delay in the control system and the disturbance from the mechanical operations. In the experimental setups, in order to provide more workspace for the probe tip in the captured frame, the resolution of captured frame from microscope is bounded between 2 and

3 μm, so when validation threshold is less than 3 μm, the average position error is hard to be improved. As discussed in the control system design, the control system cannot respond fast enough to the unexpected disturbances. Sometimes, the validation process starts to adjust the output positions when the position error is already much larger than the validation threshold. The smaller threshold also has its own limitations, which are potentially increasing the chances of repeated adjustments at the target position. Although the repeated adjustments do not have any effects on the output precision, the whole operation process can be slowed down because of the increased number of validation processes. From the results in Table 5.7. using 5 μm as the validation can guarantee not only the overall performance on the precision of output movement but also the relatively faster operation speed. Figure 5.8 shown below demonstrates the position error tests with different sizes and shapes of trajectories. The size of the trajectory is considered as a potential factor which can affect the precision of output performance. Table 5.8 and 5.9 demonstrate the output position errors for different size of trajectory. For both square and circular trajectory, the output position errors do not increase or decrease as the size of trajectory increase. This phenomenon also can be found in Figure 5.9. The average position error stays around 1.4 μm when the validation threshold is at 5 μm, so the size of the trajectory does not affect the output precision.

Table 5.4. Average step length calibration for 100 μm increment

Trial number	Number of step	Resolution per step [μm/step]
1	132	0.758±0.015
2	133	0.752±0.015
3	130	0.769±0.015
4	136	0.735±0.015
5	137	0.730±0.015

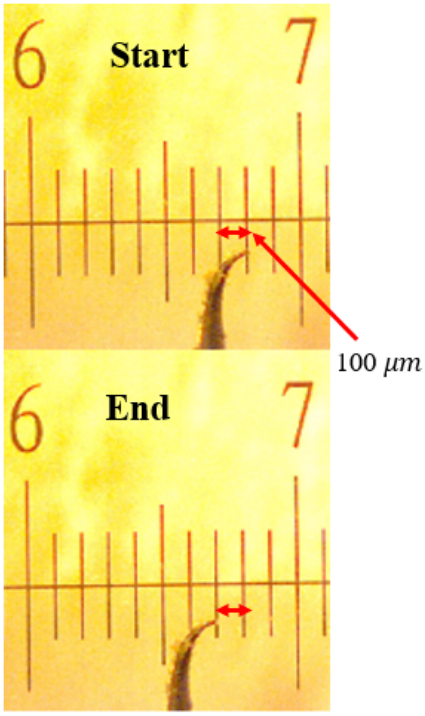

Figure 5.6. Resolution tests.

Table 5.5. Results of square trajectory tests

Square(W = 400 μm)	Trial1[μm]	Trial2[μm]	Trial3[μm]	Trial4[μm]	Trial5[μm]
Average error	1.50	1.22	1.46	1.68	1.47
Standard deviation	0.64	0.68	0.62	0.59	0.58
Maximum error	6.8	6.2	6.4	6.6	5.7

Table 5.6. Results of circular trajectory test

Circle(D = 400 μm)	Trial1[μm]	Trial2[μm]	Trial3[μm]	Trial4[μm]	Trial5[μm]
Average error	1.23	1.34	1.37	1.52	1.34
Standard deviation	0.94	0.88	0.97	0.92	0.96
Maximum error	6.5	6.4	6.7	6.3	6.4

Table 5.7. Performance with different validation threshold

Threshold	10 [μm]	7 [μm]	5[μm]	3[μm]	1[μm]
Average position error	4.37	2.84	1.63	1.57	1.48
Maximum position error	12.8	8.2	6.5	5.4	5.4

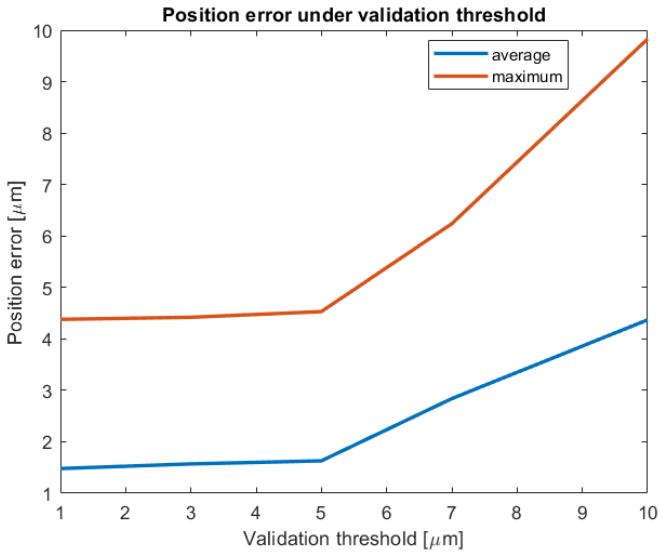

Figure 5.7. Average position error at different position error.

Table 5.8. Output performance of different size of square trajectory

Square	Trial1[μm]	Trial2[μm]	Trial3[μm]	Trial4[μm]	Average[μm]
W = 400μm	1.34	1.26	1.45	1.37	1.35
W = 600μm	1.45	1.28	1.30	1.24	1.32
W = 800μm	1.42	1.29	1.37	1.40	1.37
W = 1200μm	1.37	1.26	1.47	1.25	1.34

5.4 Speed Tests

As discussed in the previous section, the disturbances from the mechanical design have effects on the precision of output motions. It is hard to calibrate and quantify

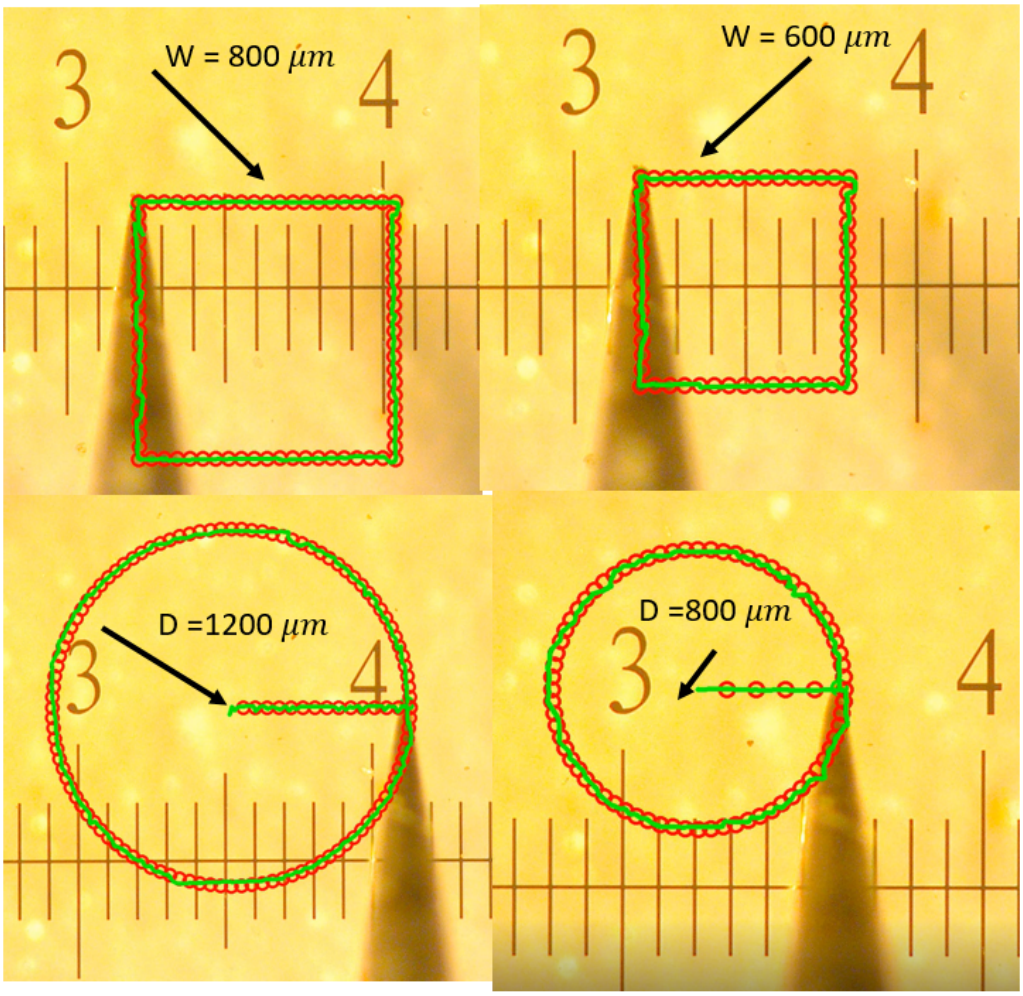

Figure 5.8. Demonstrate the performances in position error test.

Table 5.9. Output performance of different size of circular trajectory

Circle	Trial1[μm]	Trial2[μm]	Trial3[μm]	Trial4[μm]	Average[μm]
D = 400μm	1.43	1.38	1.42	1.35	1.40
D = 600μm	1.44	1.39	1.38	1.32	1.38
D = 800μm	1.41	1.43	1.37	1.33	1.38
D = 1200μm	1.35	1.44	1.37	1.39	1.39

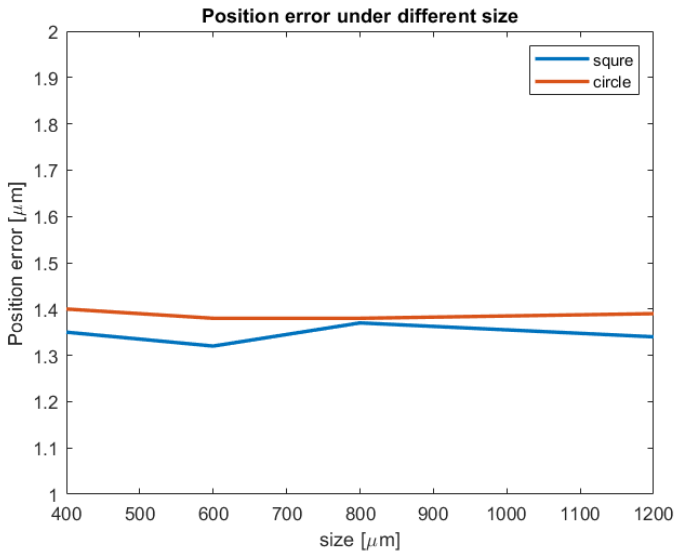

Figure 5.9. Output accuracy for different sizes of trajectory.

the values of disturbances under different working conditions, so all the factors can potentially impact the disturbance need to be analyzed through some experimental tests. The operation speed is one of the major reasons varies the disturbance in the design, so several speed tests are performed to analyze the relationship between the operation speed and output performance. The validation threshold for each speed tests remains at 5 μm. The speed tests also can be divided into two types, which are straight line tests and curved line tests. The straight line tests are performed by following the rectangular trajectory, and curved lines tests are performed by following the circular trajectory. The operation speed is controlled by the parameters of the built-in control module in the actuator. There is a parameter of controlling the desired time to reach the target position called time parameter. The changes in the time parameter in the control module can vary the operation speed. After changing the time parameter, the actual speed of output movement needs to be calibrated, so the speed tests require two steps, which are the speed calibrations, and position error calibrations. The calibrated speed can be computed by dividing the measured movement distance by the recorded time. Table 5.10 shows the relationship between

the time parameter in the control module and measured movement speed. In the table, it is obvious that the measured speed increase as the time parameter in the control module decrease. The position errors for each trajectory test are automatically generated to the external files. The position errors are calibration in both x and y-direction, because the disturbance in each dimension may vary due to different workloads.The results of position errors on x and y-dimension are shown in Table 5.11 and 5.12. The average position errors in both x and y-direction start to increase as the operation speed increases. When the operation speed reaches 78 μm/s, the average position error is already close to the validation threshold, which means that many large deviations happen during the operations. Figure 5.10 is a demonstration of how position errors change in two dimensions under different operating speeds. The errors from the y-dimension are always larger than the error from the x-dimension. one of the possible reasons causes this phenomenon is that y-dimensional component located at the bottom of the design carries the heaviest workload, which can lead to some unexpected disturbance. In the figure, when the speed is over 50 μm/s, the position error starts to dramatically increase. if the tasks do not have any requirements on operation speed, it is better to keep the operation speed lower than 50 μm/s. The purpose of Figure 5.11 is to show the differences on output performance in two different speeds. The bad output performances easily happen when the operating speed is high.

Table 5.10. The relationship between the time parameter and measured speed

Time parameter[μs]	Trial1[μm/s]	Trial2[μm/s]	Trial3[μm/s]	average [μm/s]
50	25.46	24.87	26.21	25.51
25	48.62	52.68	50.08	50.46
20	58.21	59.72	60.98	59.64
15	78.34	76.94	78.57	77.95

Table 5.11. The average position errors in x-dimension under different speeds

Speed[μm/s]	Trial1[μm]	Trial2[μm]	Trial3[μm]	average [μm]
25.5	1.50	1.22	1.46	1.39
50.5	2.10	2.46	1.8	2.12
59.4	3.66	2.42	3.46	3.18
78.0	6.10	4.01	3.62	4.58

Table 5.12. The average position errors in y-dimension under different speeds

Speed[μm/s]	Trial1[μm]	Trial2[μm]	Trial3[μm]	average [μm]
25.5	1.68	1.75	1.71	1.71
50.5	1.76	2.78	2.22	2.25
59.4	3.8	3.46	3.30	4.58
78.0	5.74	5.84	5.87	5.81

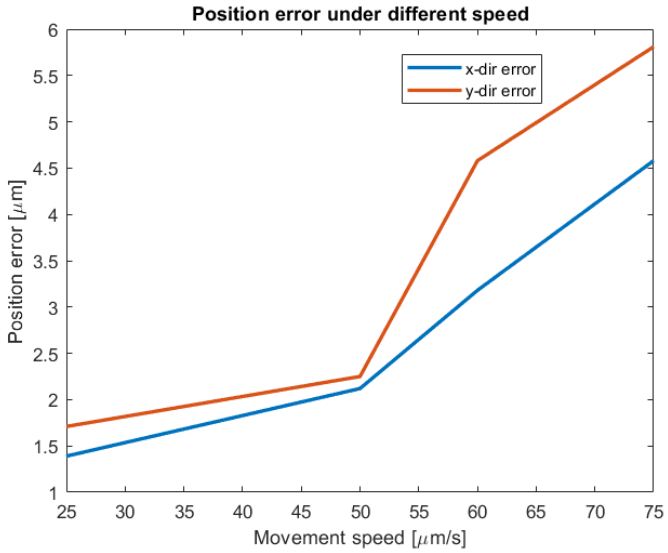

Figure 5.10. Average position error in x and y-dimension under different speeds

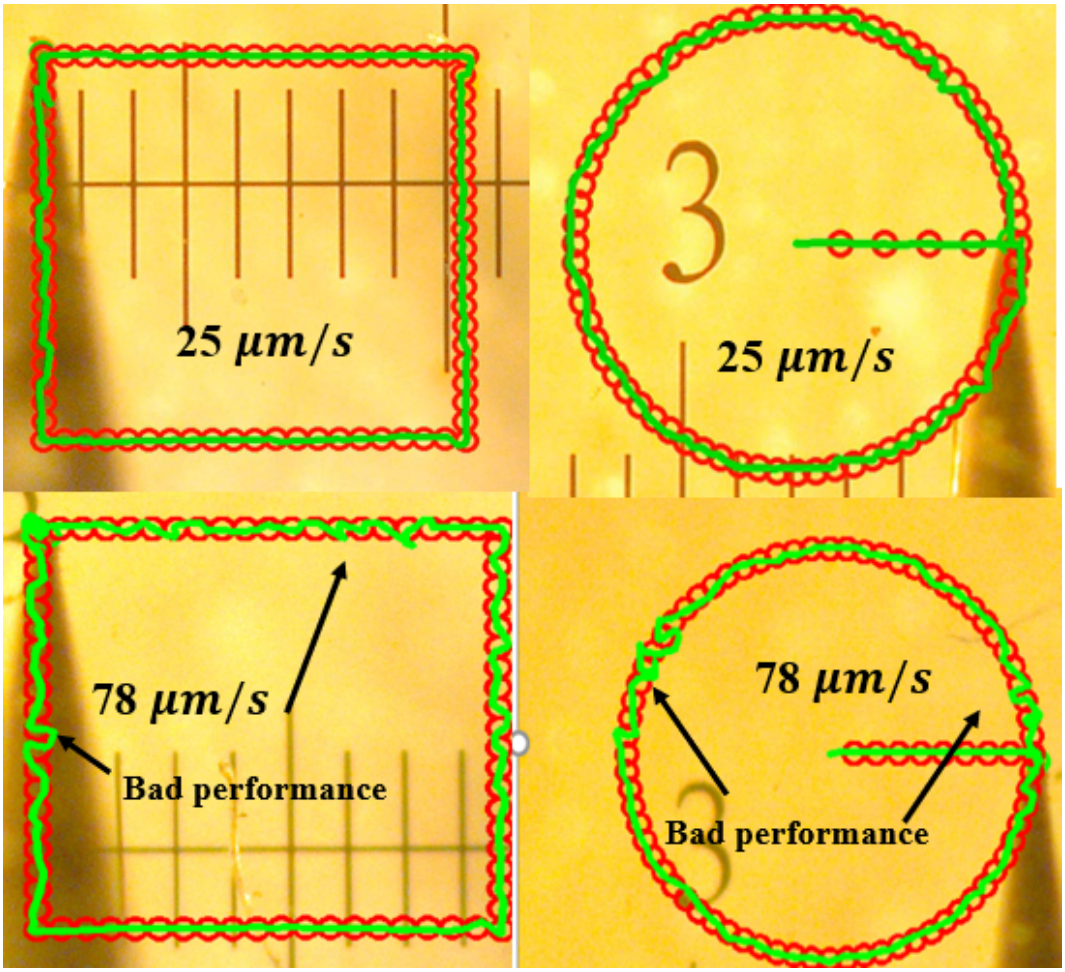

Figure 5.11. Comparison on output performance under two different speeds

5.5 Performance Test

In the previous experimental tests, all the test cases are the regular trajectory, like rectangle and circle. In order to check if the design can handle most of working conditions and environments, the irregular trajectory needs to be tested to check if the design still can accomplish the tasks in high-precision. One of the test cases is about drawing the P shape in different sizes. Figure 5.12 is the output performances for different size of P shape. The dimensions of each P is labeled in the figure. From left to right, the size of the P trajectory increase. In each test case, the output movement follows the way points accurately and steadily. The next performance test

is to manipulate the tip of probe to push a 400×400 μm micro-sample. The control system can not only draw the movement of the tip but also record the trajectory of the micro-sample. In these manipulation tests, only one micro-manipulator is used, so it is difficult to maneuver the micro-sample to follow a desired trajectory. These tests only want to demonstrate that the design can do some simple micro-manipulation tasks, like pushing the sample in a desired direction and changing the orientation of the sample.

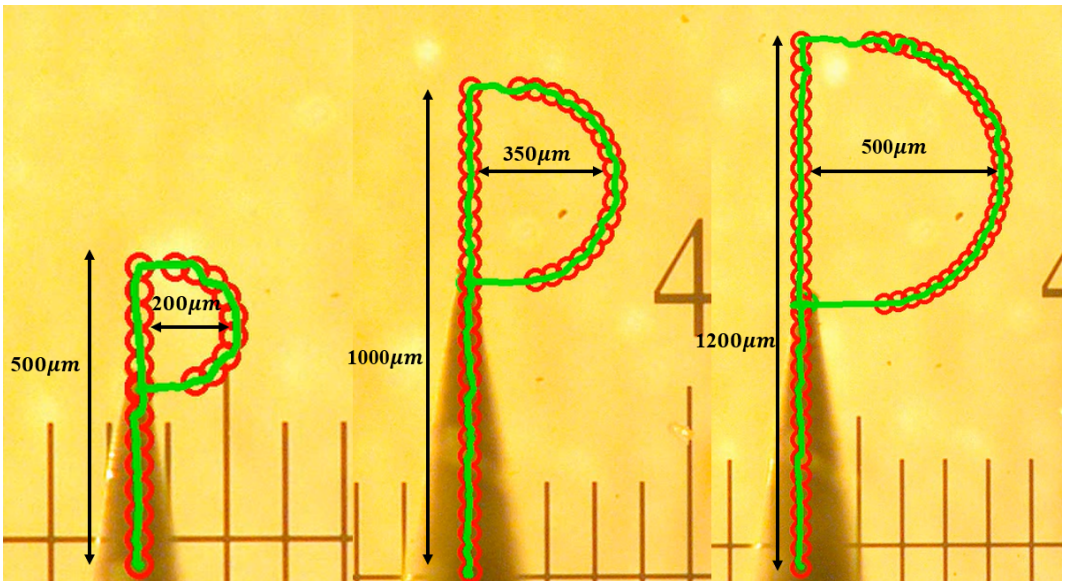

Figure 5.12. The output performance for different size of P shape

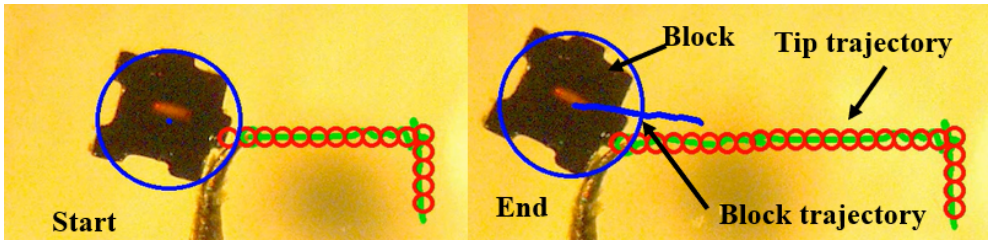

Figure 5.13. Push the block to the left

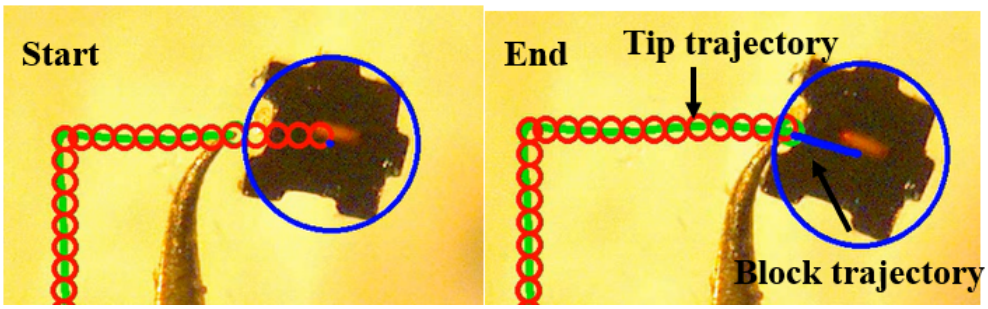

Figure 5.14. Push the block to the right

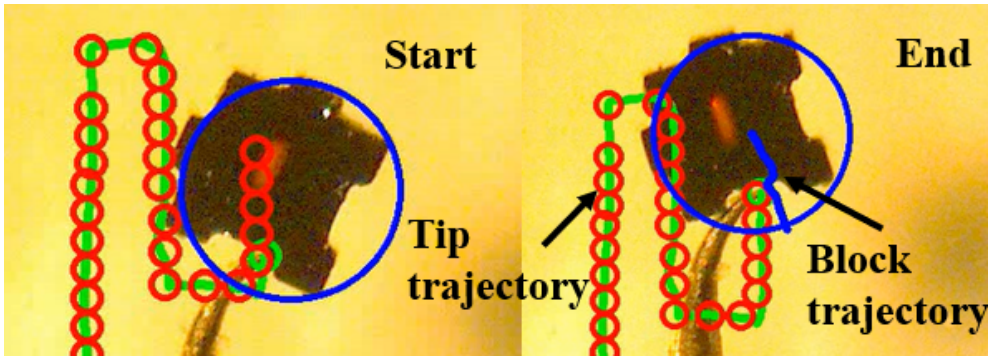

Figure 5.15. Push the block to the top

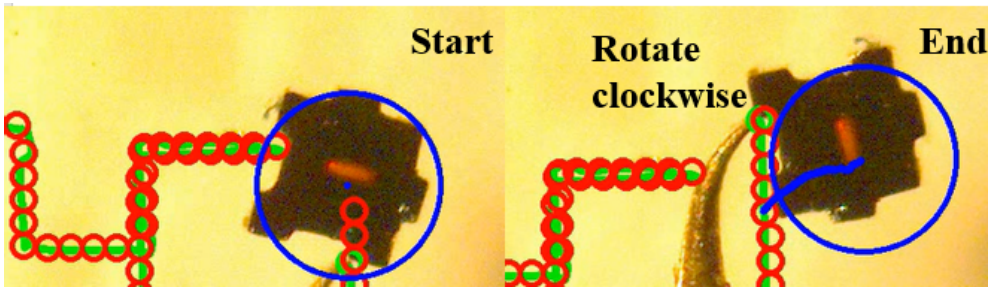

Figure 5.16. Change the orientation of the block

5.6 Experimental Results Conclusion

In this chapter, many types of experimental tests are performed to analyze and validate the performance of the design. The tests include different size of trajectory, different shapes of trajectory, different operation speeds, different validation thresh-

olds, and micro-assembly tests. In each tests, design can provide very reliable and accurate performance. All the test results are concluded in the Table 5.13.The error validation threshold is still 5 μm for all the test results shown below. These specifications of the actual design can be used to check the achievements of the design requirements. Also, these specifications of the design can be compared with specifications of benchmarks.

Table 5.13. Specifications of the design

Travel range(X)	31.8mm
Travel range(Y)	31.8mm
Travel range(Z)	31.8mm
Minimum step size	0.750$\pm$0.015 μm/step
Coarse step size	2 μm/step
Speed range	25 – 50 μm/s
Price	$550.56

6. CONCLUSION AND FUTURE WORK

The design of a mechanical system and a control system for a low-cost micromanipulator are presented. This paper consist three main parts, which are mechanical design, control system design and experimental validation. In the mechanical system, the strategies and specifications of the mechanical design are elaborately explained and analyzed. The total fabrication cost of the design demonstrated in the section of BOM is $ 550.65, which meets the design requirement for the cost. A good mechanical design is only foundations in the whole system. It also requires help from the control system to motorize and optimize the output movements in each degree of freedom. The Chapter of Control System Design lists several features which can improve the output performance and mitigate the drift motions and unexpected disturbance. Among these features, the calibration, error validation process, and way points generation are the three critical features which have large effects on the output precision. These three features are well-explained in the Chapter of Control System Design. The rest of the features are designed to provide the convenience for the users, like manual keyboard control, mouse click control, and recording position errors. These features work together to achieve teleoperated and semi-autonomous control mode. Each feature mentioned in the control system design needs to be validated its performance through experimental tests in the Chapter of Experimental Validation. Before any experimental tests, the specifications of the assembled prototype is measured to compare with the theoretical specifications shown in the Chapter of Mechanical Design. Also, the experimental setup and instruction manual of the control system are introduced to make sure that users perform the experimental tests appropriately during the experimental tests. The purposes of the experimental tests are to validate the resolution, accuracy, output performance and the limitations of the design. The design has two types of step sizes, which are coarse step size and ultra-fine step size. The

coarse setp size(2μm/step) is limited by the perception resolution(2μm/pixel). The ultra-fine step size(0.76μm/step) is theoretical value ,which is cannot be quantified by the current experiment setup. During the validation test for the resolution, the average minimum step length are computed instead. The computed average minimum step length is quite close to the theoretical minimum step size. Both types of step size meet the requirement of resolution. Some other validation tests are performed to find out factors may potentially vary the output precision, like disturbance, speed, validation thresholds, and size of trajectory. These validations tests conclude that the suggested operation speed for the design range from 25 μm/s to 50 μm/s and the appropriate validation threshold is 5 μm. With the existence of the validation process, the average output precision is bounded within 5μm, which is also meet the design requirements. The shape and size of trajectories do not have much effects on the output accuracy based on the experimental results. Some justifications are provided in the section of experimental validation to prove that the deviations on the z-dimensional movements cannot be compensated by the validation process. In order to avoid the interference with other processes during the z-dimensional movement, the tip needs to keep at least 150 μm away from other objects before any z-dimensional movements. This is one of limitations in the control system during the operation. The ultimate goal of the design is to do some micro-manipulation, like maneuvering the targeted objects to a desired position. These micro-manipulation tasks are performed to test the control system can maintain its performance in most of working conditions. Although using one designed micro-manipulator is difficult to maneuver the block steadily, the micro-manipulator prove its ability to move the micro-sample in different directions and orientations during these micro-manipulation tests. Overall, the results in these validation tests prove that all the design requirements listed at the beginning of the report are accomplished.

Currently, the design is not perfect, and there are still lots of things need to be improved. At the end of the Chapters of the Mechanical Design and Control System, the limitations are mentioned in each chapter. In the mechanical design, using 3D

printed components potentially affect the accuracy of the output performance, because the 3D printed components suffer from the problem of dimensional accuracy. The dimensions of printed components do not match up with the simulated model, so this problem can lead to the nonuniform and unsteady output movement. A possible solution is to find a more accurate solution to manufacture the prototype to reduce the possibility of unsteady motion. The limitation of the z-dimensional movement can benefit from this solution. Another big limitation is the time delay in the control system. As introduced before, the time delay is the most critical factor which leads to the loss of the accuracy on the output movement. The time delay means that the control system cannot respond fast enough to the unexpected disturbance, so the output accuracy becomes worse with the existence of the time delay. The potential solution to reduce the time delay is to design a new control module for the electric motor instead of using the built-in control module. However, program a new control module requires lots of extra works, like identification of the motor, controller design, and cogging force compensation. The new controller should be able to adjust the movements of the motor simultaneously based on the tip movements and continuously send the feedback signal to the microcontroller. This solution can effectively reduce the time delay and improve output accuracy. The last major limitation is on object tracking. The algorithms for objects tracking in this control system cannot robustly and accurately detect the target objects after huge changes in the working environment. A more robust method is using machine learning to do the image segmentation. Image segmentation is effective and accurate to separate the probe from the capture frame. This new method can improve the robustness of the control system.

REFERENCES

REFERENCES

[1] Burisch A, Wrege J, Raatz A, and Hesselbach J. PARVUS-miniaturized robot for improved flexibility in micro production. *Journal of Assembly Automation*, pages 65–73, 2007.

[2] Irene Fassi and Giovanni Legnani. Design of a Tendon Driven Parallel Manipulator for Micro-factory Applications. *ISR*, 2010.

[3] Y. Okazaki, N. Mishima, and K. Ashida. Microfactory Concept, History, and Developments. *ASME Journal of Manufacturing Science and Engineering*, 126:837–844, 2004.

[4] Bradley J. N., Lixin D., and Fumihito A. *Springer Handbook of Robotics, Part B:18.Micro/Nanorobots*. Berlin Heidelberg: Springer-Verlag, 2008.

[5] Giuseppe Carbone, Conghui Liang, and Hao Gu. Design and Simulation of a Binary Actuated Parallel Micro-Manipulator. *13th World Congress in Mechanism and Machine Science*, 2011.

[6] Bob Hayward, David Moschella, Jon Schreiber, Simon Wardley, and Howard Smith. 3D printing and the future of manufacturing . *CSE*.

[7] Medhavi Kamran and Abhishek Saxena. A Comprehensive Study on 3D Printing Technology . *MIT International Journal of Mechanical Engineering*, 6:63–69, 2016.

[8] Chris Anderson. Makers: The new industrial revolution. *New York: Crown Business*, page 210, 2012.

[9] H. N Savia, M.and Koivo. Contact Micromanipulation Survey of Strategies. *IEEE/ASME Trans. Mechatronics*, 14(4):504–514, 2009.

[10] J. T. Feddema, P. Xavier, and R Brown. Micro-Assembly Planning With Van Der Waals Force. *IEEE International Symposium on Assembly and Task Planning*, pages 32–38, 1999.

[11] Y. Zhou and B. J Nelson. The Effect of Material Properties and Gripping Force on Micrograsping. *IEEE International Conference on Robotics and Automation*, pages 1115–1120, 2000.

[12] C Keller. Microgrippers With Integrated Actuator and Force Sensors. *World Automation Congress*, pages 217–222, 1998.

[13] R. S Fearing. Survey of Sticking Effects for Micro Parts Handling. *IEEE/RSJ International Conference on Intelligent Robots and Systems. Human Robot Interaction and Cooperative Robots*, pages 212–217, 1995.

[14] S. Y. Nof. *Handbook of Industrial Robotics, 2nd ed.* Wiley Sons, New York, 1999.

[15] YU ZHOU, BRADLEY J. NELSON, and BARMESHWAR VIKRAMADITYA. Integrating Optical Force Sensing with VisualServoing for Microassembly. *Journal of Intelligent and Robotic Systems*, 28:259–276, 2000.

[16] D. Arai, F.and Ando and T Fukuda. Micro manipulation based on micro physics strategy basedon attractive force reduction and stress measurement. *1995 IEEE/RSJ Internat.Conf. on Intelligent Robots and Systems*, 2:236–241, 1995.

[17] Cappelleri, P.and Fink J.and Gavrea B.and D. J., Cheng, and V. Kumar. Automated Assembly for Mesoscale Parts. *IEEE Trans. Autom. Sci. Eng*, 8(3):598–613, 2011.

[18] M.T. Mason, A.D. Christiansen, and T.M. Mitchell. Experiments in robot learning. *In Proceeding of the Sixth International Workshop on Machine learning*, pages 141–145, 1989.

[19] Y.and Hirokazu K.and Yasumichi A. Maeda and Tamio A. Planning of Graspless Manipulation by Multiple Robot Fingers. *IEEE International Conference on Robotics and Automation, Seoul, South Korea, May 2126*, pages 2474–2479, 2001.

[20] M. T Mason. Manipulator Grasping and Pushing Operations. *Massachusetts Institute of Technology*, 1982.

[21] S.and Stolkin R.and Mcorwald T. Kopicki, M.and Zurek and J Wyatt. Learning to Predict How Rigid Objects Behave Under Simple Manipulation. *IEEE International Conference on Robotics and Automation, Shanghai, China May 913*, pages 5722–5729, 2011.

[22] J.-S. Song, P.and Pang and R. V Kumar. A Semi-Implicit Time-Stepping Model for Frictional Compliant Contact Problems a Semi-Implicit TimeStepping Model for Frictional Compliant Contact Problems. *Int.J*, 60(13):2231–2261, 2004.

[23] Berard-S. Trinklet, J. C. and J. S Pang. A Time-Stepping Scheme for Quasistatic Multibody Systems. *IEEE International Symposium on Assembly and Task Planning, Montreal, Quebec, Canada*, pages 19–21, 2005.

[24] Sutter Instrument. *STAND-ALONE MANIPULATORS.* `https://www.sutter.com/MICROMANIPULATION/mp225.html`.

[25] L.Hao, Mingyao Lin, DaXu, NianLi, and Wei Zhan. Cogging Torque Reduction of Axial-Field Flux-Switching Permanent Magnet Machine by Rotor Tooth Notching. *IEEE Transactions on Magnetics*, 51(11), 2015.

[26] K. Varanasi, Kripa Nayfeh, and Samir. The Dynamics of Lead-Screw Drives: Low-Order Modeling and Experiments. *Journal of Dynamic Systems Measurement and Control-transactions of The Asme - J DYN SYST MEAS CONTR*, 2004.

[27] Geir Hovland, S Hanssen, Stig Moberg, T Brog, Svante Gunnarsson, and Mats Isaksson. Nonlinear Identification of Backlash in Robot Transmissions. 2019.

[28] Tadeo A. T and Katia Cavalca. A comparison of flexible coupling models for updating in rotating machinery response. *Journal of the Brazilian Society of Mechanical Sciences and Engineering*, 2003.

[29] Budynas.R and Nisbett.K. *Shigley's Mechanical Engineering Design , 8th ed.* McGraw-Hill, 2008.

[30] Oberg.E, Jones.D.J.and Holbrook L.H, and Ryffel H.H. *Machinery's Handbook , 26th ed.* Industrial Press Inc, 2000.

[31] Collins J.A.and Busby H.R.and Staab G.H. *Mechanical Design of Machine Elements and Machines, 2nd ed.* John Wiley Sons, 2000.

[32] Arduino. *ARDUINO MEGA 2560 REV3.* `https://store.arduino.cc/usa/mega-2560-r3`.

[33] Shady Farah. Physical and Mechanical Properties of PLA,and Their Functions in Widespread Applications A ComprehensiveReview. *Advanced Drug Delivery Reviews,*, 107, 2016.